Title

AAVshRNA-mediated PTEN knockdown in adult neurons attenuates activity-dependent immediate early gene induction

Authors

Steward, Oswald
Coulibaly, Aminata P
Metcalfe, Mariajose
et al.

Publication Date

2020-04-01

DOI

10.1016/j.expneurol.2019.113098

Peer reviewed

HHS Public Access

Author manuscript

Exp Neurol. Author manuscript; available in PMC 2021 April 01.

Published in final edited form as:

Exp Neurol. 2020 April ; 326: 113098. doi:10.1016/j.expneurol.2019.113098.

AAVSHRNA-MEDIATED PTEN KNOCKDOWN IN ADULT NEURONS ATTENUATES ACTIVITY-DEPENDENT IMMEDIATE EARLY GENE INDUCTION

Oswald Steward[1,2,3,4,5], **Aminata P. Coulibaly**[*,1,2,5], **Mariajose Metcalfe**[1,2,5], **Jennifer M. Yonan**[1,2,5], **Kelly M. Yee**[1,2,5]

[1]Reeve-Irvine Research Center and Departments of University of California Irvine

[2]Anatomy & Neurobiology, University of California Irvine

[3]Neurobiology & Behavior, and University of California Irvine

[4]Neurosurgery, University of California Irvine

[5]School of Medicine, University of California Irvine

Abstract

Genetic deletion or knockdown of *PTEN* enables regeneration of CNS axons, enhances sprouting of intact axons after injury, and induces *de novo* growth of uninjured adult neurons. It is unknown, however how PTEN deletion in mature neurons alters neuronal physiology. As a first step to address this question, we used immunocytochemistry for activity-dependent markers to assess consequences of PTEN knockdown in cortical neurons and granule cells of the dentate gyrus. Adult rats received unilateral intra-cortical injections of AAV expressing shRNA against PTEN and were allowed to survive for 2 months. Immunostaining for c-fos under resting conditions (home cage, HC) and after 1hr of exploration of a novel enriched environment (EE) revealed no hot spots of c-fos expression that would suggest abnormal activity. Counts revealed similar numbers of c-fos positive neurons in the area of PTEN deletion vs. homologous areas in the contralateral cortex in the HC and similar induction of c-fos with EE. However, IEG induction in response to high frequency stimulation (HFS) of the cortex was attenuated in areas of PTEN deletion. In rats with AAVshRNA-mediated PTEN deletion in the dentate gyrus, induction of the IEGs c-fos and Arc with HFS of the perforant path was abrogated in areas of PTEN deletion. Immunostaining using phosphospecific antibodies for phospho-S6 (a downstream marker for mTOR activation) and phospho-ERK1/2 revealed abrogation of S6 phosphorylation in PTEN-deleted areas but preserved activation of phosphosphorylation of ERK1/2.

Corresponding Author: Oswald Steward, Ph.D., Reeve-Irvine Research Center, 837 Health Sciences Dr., University of California Irvine School of Medicine, Irvine, CA 92697, osteward@uci.edu.

[*]Current address: Department of Neuroscience, University of Virginia School of Medicine, Charlottesville, VA, 22901

Author contributions: OS designed research, all authors performed research and analyzed data.

Conflict of interest: OS is a co-founder and has economic interests in the company “Axonis”, which holds a license on patents relating to *PTEN* deletion and axon regeneration.

Keywords

Sensorimotor cortex; hippocampus; dentate gyrus; perforant path; AAV-shRNA; PTEN; immediate early gene; IEG; c-fos; phosphatase and tensin homolog; mTOR; ribosomal protein S6; MAP kinase; ERK1/2; phospho-specific antibodies

INTRODUCTION

The tumor suppressor gene phosphatase and tensin homolog (*PTEN)* has been identified as a major negative regulator of neuronal growth in the adult brain. Deletion of *PTEN* enables axon regeneration and enhances sprouting after a variety of CNS injuries (He and Jin 2016). The initial discovery was that conditional genetic deletion of *PTEN* in the retina enabled regeneration of axons from retinal ganglion cells after optic nerve crush via activation of mTOR (Park et al. 2008). Subsequent studies documented that deletion of *PTEN* in the sensorimotor cortex enabled regeneration of corticospinal tract (CST) axons following spinal cord injury (Liu et al. 2010). Regenerative growth of CST axons can also be achieved via AAVshRNA knockdown of *PTEN* in the sensorimotor cortex of adult rats (Lewandowski and Steward 2014). In addition to enabling regeneration, *PTEN* deletion converts adult cortical neurons to a juvenile state in which there is *de novo* growth of cell bodies and dendrites (Gallent and Steward 2018). The consequences of persistent activation of mTOR and ongoing growth on the physiological operation of neurons embedded in functional circuits in the mature brain are unknown.

Previous studies of consequences of *PTEN* deletion during early development have documented physiological abnormalities once neurons mature. *PTEN* deletion in adult-born dentate granule cells by tamoxifen driven CRE expression led to neuronal hypertrophy, increased numbers of dendritic spines and development of spontaneous seizures that increased in severity over time (Pun et al. 2012). Deletion of *PTEN* at postnatal day 30 in *Nestin-CreER*^{T2}PTENff mice also led to cellular hypertrophy, with occasional generalized seizures (Amiri et al. 2012). Physiological studies of consequences of *PTEN* deletion in adult born dentate granule cells reveal higher membrane capacitance, lower input resistance, increased threshold current and lower threshold voltage in *PTEN* deleted neurons compared to controls (Williams et al. 2015).

The above studies suggest that the loss of PTEN protein may alter neuronal physiology and synaptic signaling, but it is not known how PTEN deletion in fully mature neurons would affect how neurons operate in circuits. To begin to explore whether neurons lacking PTEN exhibit normal circuit activation, we assessed immediate early gene (IEG) induction, which marks neurons that have recently exhibited intense activity, for example during a seizure, or that have been engaged during learning experiences (Vazdarjanova et al. 2002; Kitanishi et al. 2009; Farris et al. 2014). Following a seizure, expression of IEGs like *c-fos* and *Arc* persist for hours marking neurons that have participated in the seizure activity (Peng and Houser 2005). Activity-dependent IEG induction is thought to be important for long-term synaptic plasticity; thus induction of transcription is a provisional indication that neurons have are underging activity-dependent synaptic modifications.

Based on this rationale, the present study uses immunocytochemistry for c-fos and Arc to assess IEG expression in two settings: 1) In the sensorimotor cortex in which PTEN has been knocked down via AAVshPTEN in the way that enables regenerative growth of the CST after spinal cord injury (Lewandowski and Steward, 2014); 2) In the adult dentate gyrus in response to patterns of synaptic activity that strongly induce IEGs. If PTEN knockdown in adult neurons leads to abnormal excitatory activity that might trigger or pre-dispose to seizures, this should be reflected by "hot spots" of IEG expression. Conversely, if PTEN knockdown disrupts activity-induced IEG induction, this should be reflected by diminished IEG expression in response to neuronal activity. Our results reveal no hotspots of IEG expression that might indicate abnormal excitatory activity, and normal activation in response to a learning experience (exposure to a novel environment). However, IEG induction in response to intense neuronal activity such as high frequency stimulation of the cortex or perforant path is attenuated.

MATERIALS AND METHODS

AAV shRNA vectors:

The AAVshPTEN vector (serotype AAV2/9) expresses shRNA-PTEN from the human U6 promoter and a zsGreen reporter protein from the CMV promoter as previously described (Lewandowski and Steward 2014). Studies involving cortical stimulation and cell size assessment were done using a similar vector in which zsGreen was replaced by GFP. The control vector was the same AAV2/9 vector expressing shRNA against luciferase (AAVshLuc). Vectors were constructed by the University of Pennsylvania Vector Core. As previously documented, intra-cortical injections of AAVshPTEN lead to effective knockdown of PTEN in cortical neurons (Lewandowski and Steward 2014).

Animals and surgery—Experimental animals were adult female Fisher 344 rats. Some experiments involving injections into the dentate gyrus were done with Fisher 344 transgenic rats from our breeding colony that express GFP. All procedures were approved by the Institutional Animal Care and Use Committee (IACUC) at the University of California Irvine.

AAVshRNA injections into the sensorimotor cortex:

Rats were anesthetized with isoflurane (2–3%) and placed in a stereotaxic device. The scalp was incised and burr holes were drilled in the skull at 2.5L/2.0P; 2.5L/1.0P; 3.2L/1P; 2.5L/0P; and 3.2L/0P. Using a Hamilton syringe tipped with a pulled glass pipette, a total of 5X 1μl injections of AAVshRNA were made at each site at a depth of 0.8mm (total of approximately 10^9 genome copies); ten rats received the control vector (AAVshLuc). Injections were unilateral to allow comparisons between areas in which PTEN was depleted vs. the homologous area of the contralateral cortex. After completing the injections, the scalp was sutured and rats were kept on water circulating heating pads until they recovered from the anesthetic and then were returned to their home cage. Rats were allowed to survive for 8 weeks post-AAV injection.

Home cage vs. novel enriched environment (EE):

The study of basal and learning-induced IEG expression involved 20 rats that received AAVshPTEN (n=10) or AAVshLuc (n=10) and were allowed to survive for 2 months post-AAV injection. Animal numbers were based on data from previous studies in mice in which n=5 per condition provided adequate statistical power (Steward et al, 2018). Rats were divided into 2 experience groups using a random number generator. Five rats of each AAVshRNA treatment group were allowed to explore a novel enriched environment prior to sacrifice (EE). The enriched environment was a 2×2' black box with plastic toys scattered on the floor. Rats were placed individually in the box for 1 hr. At the end of the hour, rats immediately received a lethal dose of Fatal Plus (~85 mg/kg) and were transcardially perfused with 4% paraformaldehyde solution in 0.1M phosphate buffer. Home cage controls (HC), were removed from their home cage and immediately received a lethal dose of Fatal Plus® and were transcardially perfused with 4% paraformaldehyde.

High Frequency electrical stimulation of the cortex:

The study of IEG induction with cortical stimulation involved 3 rats that received AAVshPTEN injections into the cortex as above and survived for 4 months and 3 un-injected controls. For this study, we used the AAVshPTEN vector with GFP reporter. Rats were anesthetized via intraperitoneal injections of 20% urethane (1ml initial dose with supplemental doses of 0.5ml approximately every 10 minutes until the animal was unresponsive to tail pinch). Rats were positioned in a stereotaxic apparatus and burr holes were placed in the skull (anterior site: 2.5A, 2.0L; posterior site: 4.0 posterior, 3.0L). Flat-end machine screws were placed in the posterior burr hole and advanced to touch the cortical surface. An insulated wire was inserted into the cortex at the anterior position to a depth of 0.5mm. For the rats that had previously received intra-cortical injections of AAVshPTEN, the insulated wire stimulating electrode was inserted through the soft scar tissue that had formed in the craniotomy site in the skull. Stimulus intensity was set to evoke a forelimb twitch in response to a single pulse (anode at the anterior position). Then, high frequency stimulation (HFS) was delivered for 10 minutes (trains of eight pulses at 400Hz given at a rate of 1/10 seconds). Rats were allowed to survive for 20–60 minutes after after completion of HFS, and then rats received Fatal Plus® (0.5ml) and were perfused with 4% paraformaldehyde.

AAVshRNA injections into the dentate gyrus: Rats were prepared for AAV injection surgery as described above except that a single burr hole was made over the dorsal hippocampus (3.5 posterior to bregma, 1.8 lateral). A single injection of 0.3μl of AAVshRNA (total of approximately 3×10^8 genome copies) was made at a depth of 2.8mm. Fifteen female rats received AAVshPTEN; six rats received the control vector (AAVshLuc). Rats were allowed to survive for 2–5 months post-AAV injection.

Neurophysiology:

Two rats that had received AAVshRNA injections into the dentate gyrus were euthanized without neurophysiological recording to assess IEG and kinases with PTEN knockdown alone. The remainder were used for neurophysiology. Rats were anesthetized for acute

neurophysiology via intraperitoneal injections of 20% urethane and were positioned in a stereotaxic apparatus. A burr hole was placed in the skull at 4.2 mm lateral to the midline and 1.0mm anterior to the transverse sinus for placement of a stimulating electrode into the entorhinal cortex. The depth of the stimulating electrode was adjusted to optimally activate the medial perforant path originating from the medial entorhinal cortex (EC) – usually about 4mm below the cortical surface. Glass recording electrodes filled with 0.9% saline were lowered into the brain through the burr hole that was previously placed for AAVshRNA delivery and positioned in the dorsal blade of the dentate gyrus to record field potentials from the cell body layer.

Stimulation paradigm:

After positioning the stimulating and recording electrodes, stimulus intensity was set so as to evoke a population spike of 3–6 mV. Single test pulses were delivered at a rate of 1/10 seconds for 10 minutes in order to determine baseline response amplitude; measures were the slope of the population EPSP and amplitude of the population spike. Following baseline recordings, 3 rounds of high frequency stimulation were delivered at the same stimulus intensity, with each round consisting of ten trains of eight pulses at 400Hz given at a rate of 1/10 seconds. After delivering 3 bouts of HFS, test pulses were delivered at a rate of 1/30sec for 1hr to determine the extent and duration of LTP. Then, HFS was continued at a rate of one 400hz train per 10sec for 1hr to activate kinase pathways and induce IEGs. One additional rat received 3 bouts of HFS (30 trains) and survived for 1 hour. At the designated survival time, rats received Fatal Plus® (0.5ml) and were perfused with 4% paraformaldehyde for immunohistochemistry. One additional rat received 3 bouts of HFS (30 trains) and survived for 1 hour.

Tissue preparation and Immunohistochemistry (IHC) for rats that received intra-cortical injections—Brains were cryoprotected in 27% sucrose and frozen in OCT using a mixture of dry ice and 100% ethanol. Brains were sectioned in the coronal plane by cryostat collecting sets of sections at 300μm intervals.

Sets of sections were immunostained for PTEN to determine the area of PTEN knockdown, for c-fos as a measure of IEG expression and using antibodies that recognize the phosphorylated form of ribosomal proten S6 (p-S6), which is a downstream marker for mTOR activation. Prior to immunostaining, sections were placed in 1.7mL microfuge tubes with nano-pure water and microfuge tubes were placed in boiling water for 5min for antigen retrieval. Sections were then equilibrated in TBS (100mM Tris, pH 7.4 and 150mM NaCl), blocked for 1–2hrs at room temperature in 5%TSA blocking reagent (Perkin Elmer catalog FP1012) or in TBS with 5% normal donkey serum and 0.3% Triton X-100 and then incubated overnight in primary antibodies diluted in blocking buffer. Primary antibodies were rabbit anti-PTEN (1:250 Cell Signaling Technology; Cat # 9188), rabbit anti c-fos (1:1000 Millipore; ABE457) and rabbit anti-p-S6 SER 240–244 (1:250 Cell Signaling Technology; Cat # 2215). Sections were rinsed and incubated in horseradish peroxidase (HRP) conjugated donkey anti rabbit secondary (1:250; Jackson ImmunoResearch Laboratories). Sections were then treated by Catalyzed Reporter Deposition (CARD)

amplification to generate tyramide-Cy3. Sections were then washed with TBS, mounted and coverslipped using Vectashield.

Image collection and quantification of c-fos positive neurons—PTEN IHC was used to determine the area of knockdown. For rats that received AAVshPTEN injections into the cortex, a sampling box 750μm wide was positioned over the cortex in the area of PTEN deletion identified by PTEN IHC and in the homologous area in the contralateral hemisphere, which serves as an intra-animal control. C-fos positive neurons were summed across cortical layers from the cortical surface to the white matter.

Cell size measurements.

To quantify de novo growth of PTEN-depleted cortical neurons, a subset of animals (n=3) received unilateral injections of AAV-shPTEN-GFP as above and were allowed to survive for 4 months post injection. Brains were sectioned in the coronal plane at 40μm thickness on a Vibratome® collecting sets of sections at 480μm intervals. One set of sections was triple stained for PTEN immunofluorescence, NeuN and Hoechst for nuclear detection.

Sections were washed in TBS (100mM Tris, pH 7.4 and 150mM NaCl) then quenched for endogenous peroxidase activity by incubation in 3%H2O2/TBS for 15 minutes. Sections were then washed in TBS and blocked in blocking buffer (TBS, 0.3% Triton X-100, 5% NDS) for 2 hours at room temperature. Sections were then incubated overnight at room temperature in buffer containing primary antibodies for rabbit anti-PTEN (1:250, Cell Signaling Technology; 9188) and mouse anti-NeuN (1:200, Millipore MAB377). Sections were then washed in TBS, incubated for 2 hours in buffer containing biotinylated donkey anti-rabbit IgG (1:250, Jackson ImmunoResearch 711–065-152) and donkey anti-mouse Alexa 555 (1:250, Invitrogen A31570), then washed again. PTEN detection was accomplished through incubation in ABC reagent (Vectastain Elite kit, catalog #PK-6100; Vector Laboratories) and CARD amplification with Tyramide-FITC. Sections were then mounted on 0.5% gelatin coated slides and counterstained with Hoechst (1μg/mL).

Three consecutive sections spaced 480μm apart were taken for assessment of cross sectional area. Images were taken at 10x on an Olympus A×80 microscope and images were imported into ImageJ. Sampling was done by identifying a 400×300μm region of interest (ROI) in layer V of the motor cortex within the area of PTEN knockdown. PTEN deletion was confirmed by a lack of co-labeling of PTEN with NeuN. The cross-sectional area of cell bodies and corresponding nuclear size were manually traced beginning at the top left end of the ROI, moving medially until 25 cells were collected. Only neurons with a pyramidal cell shape were included, and whose soma and nuclear borders could be distinguished from surrounding cells. As an intra-animal control, 25 PTEN-expressing cells and their corresponding nuclei were measured on the contralateral cortex using comparable methods. In total, 75 PTEN-depleted and 75 PTEN-expressing neurons were assessed per animal, calculating averages for each individual rat, then the overall mean cross-sectional area for the PTEN depletion and control groups was determined by averaging measures across rats.

Tissue preparation of brains from rats that received AAVshRNA into the dentate gyrus—Brains were sectioned in the coronal plane on a Vibratome® at 40μm

collecting sets of sections at 480μm intervals and sections were stored in phosphate buffered saline (pH 7.4). Unstained sections were mounted on slides to visualize zsGreen expression. To define the area of PTEN knockdown, one set of sections was immunostained for PTEN as described above. Other sets were immunostained for *c-fos* (as above) and *Arc* and for the phosphorylated form of ribosomal protein S6 (p-rpS6) and the phosphorylated form of extracellularly regulated kinase 1/2 (p-ERK1/2).

Preparation for immunostaining and incubation in primary antibodies was as above; Primary antibodies were: rabbit anti-Arc (1:1000 Synaptic Systems 156 003); rabbit anti-c-fos, (1:1000 EMD Millipore ABE457); rabbit anti-p-rpS6 ser 240/244 (1:250 Cell Signaling 2215); rabbit anti-p-rpS6 ser 235/236 (1:250 Cell Signaling 4858); goat anti-p-ERK 1/2 (1:100 Santa Cruz Biotech SC-16982).

Sections were then incubated 1 to 2 hours in a 1:250 dilution of biotin-conjugated donkey anti-rabbit IgG (Jackson ImmunoResearch, 711–065-152) for all immunostains with the exception of the p-ERK 1/2 for which a 1:250 dilution of biotin-conjugated rabbit anti-goat IgG (Vector Laboratories, BA-5000) was used. Sections were then treated with ABC (Vector Laboratories PK-6100) for 1– 2 hours. Sets of sections were prepared for immunohistochemistry with both DAB and immunofluorescence. For DAB, sections were stained in DAB (Vector Laboratories, SK-4100) for 3–5 minutes. For immunofluorescence, CARD amplification of Cy3 labeled tyramide was run for 25 minutes. After immunostaining, sections were mounted on 0.5% gelatin subbed slides. DAB stained slides were dehydrated through washes of graded ethanol, cleared in 3 changes of xylene and coverslipped with DPX.

Image collection and quantification—PTEN knockdown in the dentate gyrus leads to de novo growth of granule cell bodies and increases in the thickness of the granule cell layer. To determine whether there were also increases in granule cell number, sets of sections from 4 rats were immunostained for NeuN and coversliped with Vectashield® with DAPI. Images were taken of the GCL layer in the middle of the area of PTEN depletion and in the homologous part of the contralateral GCL and counts were made of the number of granule cell bodies/100μm length of the GCL. For counting, images were imported into photoshop and overlaid with a grid with lines spaced at 100μm intervals. DAPI-positive nuclei within the granule cell layer were counted including nuclei that touched the grid line on the left and excluding nuclei that touched the grid line on the right.

PTEN IHC was used to determine the area of knockdown. In sections immunostained for c-fos, Arc, and p-S6, images of the dorsal leaf of the granule cell layer were taken at 40X in 3 sites: 1) On the side contralateral to the stimulation (control); 2) Outside the area of PTEN knockdown on the side of the high frequency stimulation; 3) In the area of PTEN knockdown. We then counted the number of c-fos, Arc, and p-S6-positive dentate granule cells per 100μm length of the granule cell layer.

To quantify immunostaining for p-ERK, images were taken at 20X from the same regions as above. Images were imported into ImageJ and converted to 8-bit. An ROI line was oriented perpendicular to the granule cell layer extending from the cell layer through the molecular

layer and fluorescence intensity along the ROI line was assessed averaging 5 measurements per animal.

Statistical analysis

Data on counts of c-fos and Arc-positive neurons (n=5 rats per condition) and measures of cell body and nuclear size (n=3 rats) were imported into Graphpad Prism® software and analyzed using repeated measures two-way analysis of variance (ANOVA), with post-hoc comparisons using Sidak's multiple comparisons.

Counts of granule cells per 100μm segment of the granule cell layer (GCL) were done in 4 rats exhibiting minimal damage to the granule cell layer and data were analyzed by one-way ANOVA.

RESULTS

PTEN knockdown with intra-cortical injections of AAVshPTEN/zsGreen:

In rats that received 5 injections of AAVshPTEN/zsGreen, the area of the cortex in which zsGreen is expressed can be conveniently imaged in intact brains by by epi-fluorescence illumination (Fig. 1). ZsGreen fluorescence was present over a wide area extending throughout most of the sensorimotor cortex anterior to bregma. Within the overall area of zsGreen fluorescence, some injection sites could be identified by areas of more intense fluorescence.

In coronal sections through the brain, injection sites were marked by fluorescence for zsGreen (Fig. 1C). Immunostaining for PTEN confirmed knockdown in the areas of zsGreen fluorescence (Fig. 1C&D illustrate the same section imaged for zsGreen and PTEN). In some cases, zsGreen fluorescence extended laterally along the white matter for several mm, and immunostaining for PTEN was diminished in the areas of zsGreen fluorescence. In the gray matter, zsGreen fluorescence was mainly within cells with astrocyte morphology (Fig. 1E). In the white matter, zsGreen-positive axons and some large fluorescent particles were present in the areas of the white matter with diminished PTEN staining (Fig. 1F). Although the large particles were about the size of some of the nuclei in the white matter identified by DAPI staining, most of the large particles were not DAPI-positive (not shown).

There was complete absence of PTEN expression at the center of each injection site and a penumbra with diminished PTEN expression extending for several mm from the injection. In the penumbra, neurons lacking PTEN appeared as 'ghost cells' against a background of low levels of fluorescence. Figure 1G illustrates the penumbra in a section approximately 400μm distant from the section shown in Figure 1C–F illustrating ghost cells in layers II-III and layer V and preservation of PTEN expression in layer IV. In a previous study involving conditional genetic deletion of PTEN, immuno-negative ghost cells were confirmed to be neurons by co-staining for NeuN (Gallent & Steward, 2018).

PTEN deletion triggers de novo growth of cell bodies of cortical neurons and nuclear enlargement:

To determine whether PTEN knockdown via AAV-shPTEN induces neuronal growth in the same way as conditional genetic deletion, we measured cell body size in three rats 4 months post AAV-shPTEN injection (AAVshPTEN-GFP). In sections co-stained for PTEN, NeuN and Hoechst, NeuN-positive neurons on the side contralateral to the injection were PTEN-positive (Fig. 2A). On the side of the AAV-shPTEN injection, the area of PTEN deletion was evident by the absence of PTEN immunofluorescence with preserved NeuN staining (Fig. 2B). Insets show high magnification images of a single NeuN positive neuron expressing PTEN (Fig. 2A inset) and PTEN-depleted NeuN positive neuron (Fig. 2B inset). The average soma area for PTEN-depleted neurons was almost 2-fold higher than PTEN-expressing neurons (500.12 ± 93.13 μm^2 for PTEN-depleted neurons vs. 257.96 ± 37.98 μm^2 for PTEN-positive neurons, Fig. 2C). There were corresponding increases in average nuclear area (204.13 ± 31.31 μm^2 for PTEN-depleted neurons vs. 141.25 ± 20.15 μm^2 for PTEN-positive neurons, Fig. 2D). Two-way ANOVA revealed an overall significant difference between PTEN-depleted and PTEN-expressing neurons [$F(1, 8) = 109$, $p < 0.0001$]. A plot of soma vs. nuclear size (Fig. 2E) reveals clear separation and clustering PTEN-depleted vs. PTEN expressing neurons. These results confirm that AAVshRNA-mediated PTEN knockdown in rats triggers *de novo* growth of neuronal cell bodies and nuclei.

No hot spots of c-fos expression in areas of PTEN knockdown:

We first assessed whether neurons within the area of PTEN knockdown expressed c-fos at higher levels than normal, which might indicate neuronal hyperactivity or recent seizures (Peng & Houser, 2005)( ). Immunostaining for c-fos in rats that were euthanized immediately after removel from their home cage (HC condition) revealed no hot spots of c-fos expression in the area of PTEN knockdown or elsewhere in the brain in any of the rats. Figure 3 illustrates an example of the area of PTEN knockdown as revealed by immunofluorescence for PTEN (Fig. 3A) and c-fos expression in a nearby section (Fig. 3B). Levels of labeling for c-fos in the neocortex were very low in rats in the HC condition with only a few c-fos positive neurons in layers II-IV (Fig. 3) although c-fos positive neurons were present in the allocortex (cingulate cortex dorsally and piriform cortex, not shown). C-fos positive neurons were also sparsely distributed in the pyramidal layers of the hippocampus and granule cell layer of the dentate gyrus (not shown).

A learning experience (1 hour of exploration in a novel enriched environment) induces c-fos expression in PTEN-depleted areas of the cortex.

C-fos expression was induced in many brain regions after exploration of a novel enriched environment. In the sensorimotor cortex, c-fos positive neurons were most numerous in layers II-IV and VI (Fig. 3E&F). There was no obvious difference in the number of c-fos positive neurons in the PTEN-depleted area of the cortex (Fig. 3E) vs. the homologous region on the contralateral side (Fig. 3F). The overall pattern of immunostaining was very similar in rats that received AAVshLuc. Figure 3G illustrates zsGreen expression in the area of the injection and Figure 3H illustrates the pattern of labeling for c-fos at the injection site (same section as Fig. 3G) and the homologous region on the contralateral side (Fig. 3I)

To quantify the number of c-fos positive cells, counts were made in the area of PTEN knockdown and in the homologous region on the contralateral side comparing HC vs. EE conditions (Fig. 3J). Two-way ANOVA revealed an overall significant difference between HC vs. EE conditions [F (3/16)=10.52, p<.0005], but no significant difference between PTEN depleted (ipsilateral) vs. the contralateral control [F (1/16=0.08, p=.78].

IEG induction following high frequency stimulation (HFS) of the cortex is attenuated in PTEN-depleted areas

To determine whether PTEN knockdown would affect IEG induction in response to intense synaptic activation, we used a model involving brief high frequency stimulation (HFS) of the cerebral cortex (20 msec trains at 400hz repeated 1/10 sec for 10 minutes). In control rats, 60 400hz trains strongly induces c-fos expression throughout the cortex on the stimulated side of the brain. Figure 4 illustrates c-fos labeling in a case that received unilateral HFS to the cortex for 10 minutes and survived for 40 minutes. Although stimulation was delivered to the dorsal surface of the cortex, there was robust induction throughout the rostro-caudal axis from the rostral-most tip of the frontal lobe and anterior olfactory nucleus (Fig. 4A) through the entorhinal cortex posteriorly (not shown), with comparable induction in dorsal areas such as the cingulate cortex and sensorimotor cortex and ventral areas including the piriform cortex. Similar induction was seen in other cases that were stimulated for 10min and survived for 20 and 60 minutes. Together, the 3 cases provided the controls for comparison with cases that received AAVshRNA.

To compare the extent of induction across the cortex, we counted c-fos positive neurons across cortical layers in the dorso-medial neocortex (M1 motor cortex) and the lateral neocortex (S2 sensory cortex) ipsilateral and contralateral to the stimulation (Fig. 4D &G). On the stimulated side, there were large numbers of c-fos neurons throughout layers II-IV and layer VI, with fewer c-fos positive neurons in layer V (see Fig. 4AE&G and for counts across layers). The total number of c-fos positive neurons in a column was similar in dorsal vs. lateral neocortical regions. The widespread but unilateral induction suggests that c-fos induction is mediated by propagated neuronal activity rather than the currents generated during the stimulation.

Of note, c-fos induction is absent when HFS is delivered to the cortex in rats that are anesthetized with ketamine/xylazine despite comparable muscle twitch in response to the high frequency trains (not shown). This strongly suggests that induction of c-fos is mediated by synaptic activation via NMDA receptors.

In rats that had received unilateral injections of AAVshPTEN, unilateral cortical stimulation strongly induced c-fos expression throughout the cortex on the side of the stimulation except in the area of PTEN knockdown (Fig. 5). Figure 5A illustrates a section stained for PTEN to illustrate the area of PTEN knockdown and Figure 5B illustrates a nearby section stained for c-fos (higher magnification view shown in Fig. 5C). Counts of c-fos positive neurons across cortical layers in areas of PTEN deletion in the dorso-medial neocortex vs. the lateral neocortex revealed fewer c-fos positive neurons in the area of PTEN knockdown and a loss of the laminar pattern of c-fos induction seen in areas with intact PTEN expression (Fig 5D). Counts of the total number of c-fos positive neurons across layers revealed about a 50%

reduction in the area of PTEN knockdown vs. the lateral cortex (Fig. 4E, see legend for statistics).

Induction of phosphorylation of ribosomal protein S6 with PTEN knockdown, exploration of an enriched environment, and cortical stimulation

One of the hallmarks of mTOR activation due to PTEN *knockdown* is induction of phosphorylation of ribosomal protein S6 in neurons. Indeed, S6 phosphorylation is considered to be a canonical marker for mTOR activation. With injections of AAVshPTEN into the cortex, increases S6 phosphorylation are especially evident in large pyramidal neurons of layer V, which are the cells of origin of the corticospinal tract. Fig. 5 A&B illustrate this in one rat from the HC condition above (same case as illustrated in Fig. 3A). Immunostaining for pS (p240–244) is dramatically induced in the area of PTEN *knockdown* (Fig. 5A) in comparison to the contralateral side (Fig. 5B).

Phosphorylation of ribosomal protein S6 is also induced in specific populations of neurons by exploration in a novel enriched environment (Pirbhoy et al., 2016). Indeed, immunostaining for pS6 in the rats that explored the enriched environment revealed dramatic increases in the number of pS6 positive cortical neurons in comparison to HC controls (compare Fig. 5A&B, HC with Fig. 5C&D, EE). The pattern of immunostaining in areas of PTEN knockdown (Fig. 5C), suggests that behavioral induction of S6 phosphorylation is superimposed on the increases in S6 phosphorylation due to PTEN *knockdown* (Compare Fig. 5A, PTEN *knockdown* in HC vs. Fig. 5C, area of PTEN *knockdown* in EE).

It has recently been reported that cortical stimulation that induces sprouting of CST axons also activates S6 phosphorylation (Peng and Houser 2005). Immunostaining of sections from control rats that received cortical stimulation in the present study confirmed dramatic activation of S6 phosphorylation on the side of the HFS (Fig. 5E) in comparison to the contralateral side (Fig. 5F). This is the same rat illustrated in Fig. 3. It is noteworthy that both exploration of a novel environment and cortical stimulation induce S6 phosphorylation in neurons in different cortical layers including layer V. This is in contrast to the situation with c-fos, where few neurons in layer V are c-fos positive (see Fig. 3).

Immunostaining for pS6 in rats with AAVshPTEN injections that received cortical stimulation revealed the expected increases in S6 phosphorylation due to PTEN *knockdown* (Fig. 5G). It was not clear, however, whether there was additional activation due to HFS. Indeed if anything, it appeared that there might be fewer pS6 positive neurons than in control rats with HFS alone. Quantitative assessment is compromised however by several factors including the variable area of PTEN knockdown, local damage and potential cell loss due to the injections, and the variable distribution of pS6 positive neurons of different types across cortical layers in the area of PTEN knockdown. Because of these caveats, we switched our attention to the dentate gurus to focus on a single neuron type.

PTEN knockdown in the dentate gyrus to assess synaptically-driven IEG induction

Although it is likely that IEG induction with HFS of the cortex is driven by synaptic activity, the actual patterns of synaptic activation produced by direct cortical stimulation are not well-defined and are likely to be complex. Accordingly, we assessed whether PTEN knockdown

would attenuate IEG induction in the well-characterized model system provided by perforant path projections to the dentate gyrus. This is a useful model system because the patterns of synaptic activation can be precisely controlled and consequences of synaptic activity on IEG induction and signaling pathway activation in target neurons (dentate granule cells) are well documented (Zareen et al. 2018; Chotiner et al. 2010; Pirbhoy, Farris, and Steward 2016).

Injections of AAVshPTEN into the dentate gyrus transfected cells in an area approximately 1–2 mm in diameter as revealed by zsGreen expression (Fig. 7A). Of note, both neurons in the cell layers and cells of astrocyte morphology in the molecular layer were zsGreen-positive. Immunostaining for PTEN revealed essentially complete knockdown of PTEN protein at the injection site (Fig. 7B, same section as Fig. 7A). There were dramatic increases in size of dentate granule cell bodies and increases in the thickness of the granule cell layer in the area of PTEN knockdown, which were evident in sections stained for NeuN (Fig. 7C). Immunostaining for pS6 (a downstream marker of mTOR activation) revealed pS6-positive neurons in the area of PTEN knockdown, including large neurons in the granule cell layer and neurons in the hilus and CA1 region (Fig. 7D). It is noteworthy, however, that most PTEN-negative dentate granule cells did not show high levels of fluorescence for pS6.

One complication is that even very small injections of fluid into the dentate gyrus can cause a tissue separation at the boundary between the granule cell body layer and the hilus. This separation amputates the axons from the granule cell body and leads to degeneration of axotomized granule cells leading to a focal area of granule cell loss (Vietje & Wells, 1989). Areas of granule cell loss were seen in 5 of 13 rats that received injections of AAVshPTEN into the dentate gyrus and 3 of 5 cases that received AAVshLuc (not shown).

Increases in the thickness of the granule cell layer are not due to hyperplasia:

Increases in thickness of the granule cell layer could be due to increased numbers of granule cells or growth of granule cell bodies. To assess whether there was hyperplasia, we counted DAPI-stained nuclei in 100μm wide columns along the granule cell layer in the area of PTEN knockdown (dorsal blade) vs. the homologous region in the contralateral dentate gyrus (Fig. 7E&F). Although nuclei were larger and less densely packed in the area of PTEN knockdown, the number of granule cells was comparable on the PTEN-depleted vs. controls sides (Fig. 7G); thus, increases in the thickness of the layer are not due to increases in the number of granule cells. Two facts should be noted in considering these results: 1) local injections could have caused the death of some granule cells; 2) Counts did not correct for nuclear size, so the counts in the area of PTEN knockdown where nuclei are larger could over-estimate the actual number.

Activity-driven IEG induction is abrogated in *PTEN-depleted dentate granule cells*. To assess synaptically-driven IEG activation, a stimulating electrode was positioned in the entorhinal cortex to activate perforant path projections to the dentate gyrus and a recording electrode was lowered through the original burr hole to target the area of PTEN knockdown. Stimulus intensity was adjusted to elicit a population spike 3–6mv in amplitude in response to single pulse stimulation. After collecting baseline responses, 30 trains at 400hz were delivered and response amplitude was monitored for 1hr. Then, 400hz trains were delivered

every 10 sec for 1hr, which in control rats, reliably induces IEG expression in dentate granule cells.

Results from one representative case are illustrated in Figure 8. Figure 8A illustrates the area of transfection marked by zsGreen expression and Figure 8B illustrates the same section immunostained for PTEN to document the area of deletion. As expected, HFS strongly induced c-fos in dentate granule cells outside the area of depletion. This is documented in sections from the rostral hippocampus distant from the site of PTEN knockdown (Fig. 8C). In contrast, IEG induction was abrogated in the area of PTEN knockdown (Fig. 8D). The same pattern was evident in sections immunostained for the immediate early gene Arc (Fig. 8E &F).

To quantify IEG induction, we selected 3 cases in which there was a focal area of deletion and areas with intact PTEN expression visible in the same section (as in the section illustrated in Fig. 8D). Images were taken at 40X in 3 sites: 1) On the side contralateral to the stimulation (control); 2) Outside the area of PTEN knockdown on the side of the high frequency stimulation; 3) In the area of PTEN knockdown. Figure 8G–I illustrate high magnification views of c-fos positive dentate granule cells in these 3 sites and Figure 8K–M illustrate Arc-positive granule cells. Counts of c-fos and Arc-positive dentate granule cells per 100μm length of the granule cell layer confirmed robust induction of c-fos and Arc in the majority of dentate granule cells in areas outside the zone of PTEN knockdown and almost complete abrogation of induction in the area of PTEN knockdown (Fig. 8J&N). Very similar results were seen in the rat that received 30 trains of HFS and survived for 1hr (data not shown).

Synaptically-driven S6 phosphorylation is attenuated in PTEN-depleted granule cells:

Activation of IEG expression is dependent on NMDA receptor activation during HFS of the perforant path, so one possible explanation for the attenuation of activity-dependent IEG induction is a disruption of synaptic signals that trigger IEG transduction. To explore this, we used phospho-specific antibodies to interrogate synaptic activation of AKT-mTOR and MAPK/ERK1–2 in dentate granule cells, which are also dependent on NMDA receptor activation.

Immunostaining using antibodies for p-S6, the downstream marker of mTOR activation, revealed robust activation of phosphorylation (p-235–236) in the majority of dentate granule cells in portions of the dentate gyrus outside the area of PTEN knockdown (Fig. 9A and B, lateral portion of the dentate gyrus). As previously described (Pirbhoy et al., 2016), S6 phosphorylation occurs throughout the postsynaptic neuron including cell bodies and dendrites with a band of intense labeling in the middle molecular layer where synapses of the medial perforant path terminate (Fig. 9B&D). However, S6 phosphorylation was abrogated in PTEN-depleted areas of the dentate gyrus (Fig. 9B). Figure 9C illustrates high magnification views of labeling for p-S6 on the side contralateral to the stimulation; Figure 9D illustrates strong activation of p-S6 outside the area of PTEN knockdown on the side of the high frequency stimulation; and Fig. 9E illustrates labeling in the area of PTEN knockdown. As in un-stimulated rats, there were large p-S6 positive granule cells in the area of PTEN knockdown, which are probably the neurons in which S6 phosphorylation is

already induced as a result of persistent mTOR activation. However, most granule cells were not pS6-positive. Counts of pS6 positive dentate granule cells per 100μm length of the cell layer in the 3 areas illustrated in Fig. 8C–E revealed inducton of S6 phosphorylation in large numbers of granule cells outside the zone of PTEN knockdown and abrogation of induction in the area of PTEN knockdown (Fig. 9F).

Synaptically-driven ERK1/2 phosphorylation is preserved in PTEN-depleted granule cells:

The pattern of labeling for p-ERK1/2 is illustrated in Figure 9G–K (same case as for p-S6). As previously reported (Chotiner et al., 2010), HFS induced robust ERK1/2 phosphorylation occurs throughout cell bodies and dendrites (compare Fig. 9G, ipsilateral with 9H, contralateral side of the same section, and see Fig. 9I&J for high magnification views). Indeed, fluorescence intensity is actually higher in the dendritic laminae than in the cell body layer with a band of band of higher intensity labeling in the middle molecular layer, corresponding to the zone of activated synapses (Fig. 9J). In contrast to what was seen with p-S6, there was also robust induction of ERK1/2 phosphorylation in the area of PTEN knockdown (Fig. 9K).

Because fluorescence intensity was higher in the dendritic lamina, we quantified ERK1/2 phosphorylation by measuring fluorescence intensity across the cell body and dendritic laminae (Fig. 8L) rather than counting the number of p-ERK positive granule cells. Quantification revealed induction of ERK1/2 phosphorylation in the area of PTEN knockdown, although at a somewhat diminished level in comparison to areas outside the region of PTEN knockdown (Fig. 9J). Figure 8M–N illustrate quantification of average fluorescence intensity for pERK over the granule cell body layer and dendritic lamina (middle molecular layer) in 2 of the 3 rats in which IEG expression was assessed (IHC for p6 in the 3rd rat was unsatisfactory for quantification). Activation of ERK1/2 phosphorylation over the granule cell layer (GCL) was attenuated by about 35% (Fig. 8M) whereas activation over the middle molecular layer (MML) was attenuated by about 25% (Fig. 9N).

To exclude the possibility that abrogation of IEG induction and S6 phosphorylation were due to the AAV and/or shRNA rather than PTEN knockdown, we immunostained sections from rats that received AAVshLuc for IEGs (c-fos and Arc) and pS6. Figure 10A, illustrates zsGreen expression at the site of AAVshLuc transfection and Figure 10B–D illustrates robust induction of c-fos and Arc expression and activation of S6 phosphorylation throughout the dentate gyrus including in the area of zsGreen expression in the ventral blade. Similar results were seen in all 4 rats that received AAVshLuc and HFS of the perforant path.

Discussion

The goal of this study was to determine whether AAVshRNA-mediated knockdown of PTEN in cortical neurons would cause abnormal physiological activity. This question is based on previous findings that PTEN mutations in people as well as promoter-driven PTEN deletion in rodents, triggers brain overgrowth and physiological abnormalities including spontaneous seizures. Seizures are common with promoter-driven PTEN deletion in adult-

born dentate granule cells inmice and lead to early death (Pun et al., 2012). As an initial test of neuronal activation, we used immunocytochemistry for IEGs (specifically c-fos and Arc) that are induced by intense neuronal activity and learning. Our results revealed no “hot spots” of c-fos in cortical areas lacking PTEN or elsewhere in the brain. Also, there were no differences in IEG induction due to a learning experience (1hr exploration of a novel enriched environment). However, IEG induction due to high frequency stimulation of the cortex was attenuated in areas of PTEN knockdown. In addition, IEG induction in response to HFS of perforant path projections to the dentate gyrus was abrogated in areas of PTEN knockdown. In what follows, we discuss the implications and interpretations of these findings and caveats.

No indication of spontaneous seizure activity

The absence of any “hot spots” of IEG expression in areas of the cortex in which PTEN had been depleted argues against the possibility that any spontaneous seizures had recently occurred. This is especially true because IEGs remain elevated in neurons for many hours after a seizure event, in some cases for over 24hrs (Peng & Houser, 2005). The absence of hot spots of IEG expression does not exclude the possibility that spontaneous electrographic seizures occur in PTEN-depleted areas of the cortex, but doesn’t support the hypothesis either.

One caveat is that our data also reveal that synaptically-driven IEG induction is abrogated in neurons lacking PTEN. Thus, it is possible that neurons lacking PTEN actually did exhibit seizure-related discharge, but without IEG induction. We consider this unlikely, however, because seizures, especially clinically significant ones, propagate beyond the focus of abnormal activity and would involve neurons in the penumbra of PTEN knockdown. In this case, we would expect that neurons in the penumbra that do express PTEN would show IEG induction.

No differences in IEG induction due to a learning experience

A well-characterized model for experience-dependent IEG induction is to allow rats to explore a novel enriched environment, which induces IEG expression in many brain regions including the cerebral cortex. Our data reveal comparable increases in c-fos positive neurons in areas of the cortex in which PTEN has been depleted vs. the homologous region on the contralateral side. One caveat, however, is that the extent of IEG induction in sensorimotor regions of the cortex is not as dramatic as in other brain regions such as the hippocampus, so attenuation of induction in PTEN-depleted areas might not be evident.

Attenuation of synaptically-driven IEG induction in PTEN-depleted cortical areas

Stimulation of the cortex with brief 400hz trains identical to what is typically used to induce perforant path LTP robustly activates c-fos expression throughout the cortex on the side of the stimulation. This widespread activation strongly suggests that IEG induction is triggered by propagated neuronal activity. The fact that c-fos induction is completely blocked when animals are stimulated under ketamine-xylazine anesthesia strongly supports the interpretation that activity-dependent induction depends on NMDA receptor activation. Our results reveal that induction of c-fos expression is attenuated in the areas of the cortex in

which PTEN is depleted. Although these results strongly suggest attenuation of synaptically-driven c-fos expression, the actual patterns of synaptic activity produced by direct cortical stimulation are not well-defined.

Attenuation of activity-dependent IEG induction and S6 phosphorylation in PTEN-depleted dentate granule cells with preserved activation of ERK1/2 phosphorylation:

Stimulation of the perforant path at 400hz robustly activates MAP kinase and mTOR, as well as inducing expression of IEGs including c-fos and Arc, all of which are dependent on NMDA receptor activation. Induction of IEG expression and activation of S6 phosphorylation are abrogated in areas of PTEN knockdown whereas activation of ERK1/2 phosphorylation is preserved, although at a somewhat diminished level. The robust activation of ERK1/2 phosphorylation in areas of PTEN knockdown suggests that abrogation of other activity-dependent processes is not due to a major alteration in synaptic signaling, particularly NMDA receptor activation.

One possible explanation for the lack of activity-dependent S6 phosphorylation and IEG induction is that depletion of PTEN and activation of mTOR transforms neurons to a permanent state of immaturity. The fact that PTEN-depleted neurons exhibit *de novo* growth that continues for months supports this interpretation (Gallent & Steward, 2018). Adult-born granule cells don't show activity-induced IEG expression until about 4 weeks after the neurons are born (Carlen et al., 2002, Kee et al., 2007). Also, granule cells in alpha-CAMKII +/− mice, which are "immature" on the basis of patterns of gene expression, show essentially no induction of IEG expression (Arc) after a learning experience (training in an 8-arm radial maze) whereas IEG induction is comparable to controls in most other brain regions (Matsuo et al., 2009). Thus, signaling cascades in PTEN-depleted neurons that are ungoing *de novo* growth may be similar to immature neurons.

PTEN knockdown, a learning experience, and cortical stimulation converge to activate mTOR in cortical neurons

Induction of S6 phosphorylation is considered to be a canonical marker of mTOR activation, and a hallmark of PTEN knockdown in the cortex is persistent activation of phosphorylation of ribosomal protein S6, especially in the large pyramidal neurons of layer V (the cells of origin of the CST). It has recently been reported that cortical stimulation that induces sprouting of CST axons also activates S6 phosphorylation (Zareen et al., 2018), and one possible interpretation is that PTEN knockdown and cortical stimulation converge on the mTOR signaling pathway to activate growth competence. Surprisingly, our results reveal that a learning experience (1hr exploration of a novel enriched environment) also triggers S6 phosphorylation in cortical neurons, including layer V pyramidal neurons. Indeed, 1hr exploration of a novel environment appears to be as effective at inducing S6 phosphorylation as high frequency stimulaton of the cortex. It will be of great interest to test whether repeated complex learning experiences can substitute for electrical stimulation to enhance CST axon growth after injury.

In the dentate gyrus, synaptic induction of S6 phosphorylation is attenuated in granule neurons lacking PTEN. Such attenuation was not evident in the cortex with behavioral

induction of S6 phosphorylation or with HFS, although some decrease in activation due to HFS cannot be excluded. In any case, our data do not indicate that PTEN knockdown and HFS have additive effects on mTOR activation as measured by S6 phosphorylation. This raises the interesting possibility that HFS would actually be less able to further enhance CST regenerative growth if PTEN is also knocked down.

Potential confounds

Local injections cause some injury and AAV induce a mild inflammatory response. The present experiments were done months post-injection when inflammatory processes would have largely resolved. The control AAVshLuc control documents that PTEN knockdown is critical but it cannot be excluded that persistent inflammatory processes contribute to the effects.

Relevance for regeneration therapy

Studies from several labs have documented that deletion or knockdown of PTEN enables regenerative growth of adult CNS axons in different settings (He and Jin, 2016). Indeed, regeneration resulting from PTEN knockdown is a positive control against which other regeneration-enabling interventions are compared (Wang et al., 2015, Al-Ali et al., 2017). Regeneration due to PTEN knockdown is accompanied by enhanced recovery of motor function after spinal cord injury, (Lewandowski and Steward, 2014, Danilov and Steward, 2015). With conditional genetic deletion, PTEN is absent permanently, and our results demonstrate that AAVshPTEN-mediated knockdown also deletes PTEN for many months. One possible implication is that the resulting disruption of plasticity-related signaling pathways, particularly IEG induction, may limit the degree to which PTEN-depleted neurons can participate in activity-dependent synaptic plasticity. These findings raise the intriguing possibility that functional recovery might be enhanced by restoring PTEN expression after regenerative growth has been achieved.

Acknowledgements:

Supported by NIH grant NS047718 to OS. A. Coulibaly and J. Yonan were recipients of fellowships from NIH 5T32 NS045540. We gratefully acknowledge generous donations from Cure Medical, Research for Cure, and Lone Star Paralysis Foundation. Thanks to G Gunawan for skilled stereotaxic surgery, Jamie Mizufuka for superb histological assistance and Roxanney Zhou and An N. Nguyen for help with the immunocytochemistry and analyses.

REFERENCES

Al-Ali H, Ding Y, Slepak T, Wu W, Sun Y, Martinez Y, Xu XM, Lemmon VP, and Bixby JL. 2017. ‘The mTOR Substrate S6 Kinase 1 (S6K1) Is a Negative Regulator of Axon Regeneration and a Potential Drug Target for Central Nervous System Injury’, J Neurosci, 37: 7079–95. [PubMed: 28626016]

Amiri A, Cho W, Zhou J, Birnbaum SG, Sinton CM, McKay RM, and Parada LF. 2012. ‘Pten deletion in adult hippocampal neural stem/progenitor cells causes cellular abnormalities and alters neurogenesis’, J Neurosci, 32: 5880–90. [PubMed: 22539849]

Amiri A, Cho W, Zhou J, Birnbaum SG, Sinton CM, McKay RM, and Parada LF. 2012. ‘Pten deletion in adult hippocampal neural stem/progenitor cells causes cellular abnormalities and alters neurogenesis’, J Neurosci, 32: 5880–90. [PubMed: 22539849]

Chotiner JK, Nielson J, Farris S, Lewandowski G, Huang F, Banos K, de Leon R, and Steward O. 2010. 'Assessment of the role of MAP kinase in mediating activity-dependent transcriptional activation of the immediate early gene Arc/Arg3.1 in the dentate gyrus in vivo', Learn Mem, 17: 117–29. [PubMed: 20154358]

Farris S, Lewandowski G, Cox CD, and Steward O. 2014. 'Selective localization of arc mRNA in dendrites involves activity- and translation-dependent mRNA degradation', J Neurosci, 34: 4481–93. [PubMed: 24671994]

Gallent EA, and Steward O. 2018. 'Neuronal PTEN deletion in adult cortical neurons triggers progressive growth of cell bodies, dendrites, and axons', Exp Neurol, 303: 12–28. [PubMed: 29337147]

He Z, and Jin Y. 2016. 'Intrinsic Control of Axon Regeneration', Neuron, 90: 437–51. [PubMed: 27151637]

Kitanishi T, Ikegaya Y, Matsuki N, and Yamada MK. 2009. 'Experience-dependent, rapid structural changes in hippocampal pyramidal cell spines', Cereb Cortex, 19: 2572–8. [PubMed: 19240139]

Lewandowski G, and Steward O. 2014. 'AAVshRNA-mediated suppression of PTEN in adult rats in combination with salmon fibrin administration enables regenerative growth of corticospinal axons and enhances recovery of voluntary motor function after cervical spinal cord injury', J Neurosci, 34: 9951–62. [PubMed: 25057197]

Liu K, Lu Y, Lee JK, Samara R, Willenberg R, Sears-Kraxberger I, Tedeschi A, Park KK, Jin D, Cai B, Xu B, Connolly L, Steward O, Zheng B, and He Z. 2010. 'PTEN deletion enhances the regenerative ability of adult corticospinal neurons', Nat Neurosci, 13: 1075–81. [PubMed: 20694004]

Park KK, Liu K, Hu Y, Smith PD, Wang C, Cai B, Xu B, Connolly L, Kramvis I, Sahin M, and He Z. 2008. 'Promoting axon regeneration in the adult CNS by modulation of the PTEN/mTOR pathway', Science, 322: 963–6. [PubMed: 18988856]

Peng Z, and Houser CR. 2005. 'Temporal patterns of fos expression in the dentate gyrus after spontaneous seizures in a mouse model of temporal lobe epilepsy', J Neurosci, 25: 7210–20. [PubMed: 16079403]

Pirbhoy PS, Farris S, and Steward O. 2016. 'Synaptic activation of ribosomal protein S6 phosphorylation occurs locally in activated dendritic domains', Learn Mem, 23: 255–69. [PubMed: 27194793]

Pun RY, Rolle IJ, Lasarge CL, Hosford BE, Rosen JM, Uhl JD, Schmeltzer SN, Faulkner C, Bronson SL, Murphy BL, Richards DA, Holland KD, and Danzer SC. 2012. 'Excessive activation of mTOR in postnatally generated granule cells is sufficient to cause epilepsy', Neuron, 75: 1022–34. [PubMed: 22998871]

Vazdarjanova A, McNaughton BL, Barnes CA, Worley PF, and Guzowski JF. 2002. 'Experience-dependent coincident expression of the effector immediate-early genes arc and Homer 1a in hippocampal and neocortical neuronal networks', J Neurosci, 22: 10067–71.

Williams MR, DeSpenza T Jr., Li M, Gulledge AT, and Luikart BW. 2015. 'Hyperactivity of newborn Pten knock-out neurons results from increased excitatory synaptic drive', J Neurosci, 35: 943–59. [PubMed: 25609613]

Zareen N, Dodson S, Armada K, Awad R, Sultana N, Hara E, Alexander H, and Martin JH. 2018. 'Stimulation-dependent remodeling of the corticospinal tract requires reactivation of growth-promoting developmental signaling pathways', Exp Neurol, 307: 133–44. [PubMed: 29729248]

Chotiner JK, Nielson J, Farris S, Lewandowski G, Huang F, Banos K, de Leon R, and Steward O. 2010. 'Assessment of the role of MAP kinase in mediating activity-dependent transcriptional activation of the immediate early gene Arc/Arg3.1 in the dentate gyrus in vivo', Learn Mem, 17: 117–29. [PubMed: 20154358]

Danilov CA, and Steward O. 2015. 'Conditional genetic deletion of PTEN after a spinal cord injury enhances regenerative growth of CST axons and motor function recovery in mice', Exp Neurol, 266: 147–60. [PubMed: 25704959]

Farris S, Lewandowski G, Cox CD, and Steward O. 2014. 'Selective localization of arc mRNA in dendrites involves activity- and translation-dependent mRNA degradation', J Neurosci, 34: 4481–93. [PubMed: 24671994]

Gallent EA, and Steward O. 2018. 'Neuronal PTEN deletion in adult cortical neurons triggers progressive growth of cell bodies, dendrites, and axons', Exp Neurol, 303: 12–28. [PubMed: 29337147]

He Z, and Jin Y. 2016. 'Intrinsic Control of Axon Regeneration', Neuron, 90: 437–51. [PubMed: 27151637]

Kee N, Teixeira CM, Wang AH, and Frankland PW. 2007. 'Preferential incorporation of adult-generated granule cells into spatial memory networks in the dentate gyrus', Nat Neurosci, 10: 355–62. [PubMed: 17277773]

Kitanishi T, Ikegaya Y, Matsuki N, and Yamada MK. 2009. 'Experience-dependent, rapid structural changes in hippocampal pyramidal cell spines', Cereb Cortex, 19: 2572–8. [PubMed: 19240139]

LaSarge CL, Pun RY, Muntifering MB, and Danzer SC. 2016. 'Disrupted hippocampal network physiology following PTEN deletion from newborn dentate granule cells', Neurobiol Dis, 96: 105–14. [PubMed: 27597527]

Lewandowski G, and Steward O. 2014. 'AAVshRNA-mediated suppression of PTEN in adult rats in combination with salmon fibrin administration enables regenerative growth of corticospinal axons and enhances recovery of voluntary motor function after cervical spinal cord injury', J Neurosci, 34: 9951–62. [PubMed: 25057197]

Liu K, Lu Y, Lee JK, Samara R, Willenberg R, Sears-Kraxberger I, Tedeschi A, Park KK, Jin D, Cai B, Xu B, Connolly L, Steward O, Zheng B, and He Z. 2010. 'PTEN deletion enhances the regenerative ability of adult corticospinal neurons', Nat Neurosci, 13: 1075–81. [PubMed: 20694004]

Park KK, Liu K, Hu Y, Smith PD, Wang C, Cai B, Xu B, Connolly L, Kramvis I, Sahin M, and He Z. 2008. 'Promoting axon regeneration in the adult CNS by modulation of the PTEN/mTOR pathway', Science, 322: 963–6. [PubMed: 18988856]

Peng Z, and Houser CR. 2005. 'Temporal patterns of fos expression in the dentate gyrus after spontaneous seizures in a mouse model of temporal lobe epilepsy', J Neurosci, 25: 7210–20. [PubMed: 16079403]

Pirbhoy PS, Farris S, and Steward O. 2016. 'Synaptic activation of ribosomal protein S6 phosphorylation occurs locally in activated dendritic domains', Learn Mem, 23: 255–69. [PubMed: 27194793]

Pirbhoy PS, Farris S, and Steward O. 2017. 'Synaptically driven phosphorylation of ribosomal protein S6 is differentially regulated at active synapses versus dendrites and cell bodies by MAPK and PI3K/mTOR signaling pathways', Learn Mem, 24: 341–57. [PubMed: 28716954]

Pun RY, Rolle IJ, Lasarge CL, Hosford BE, Rosen JM, Uhl JD, Schmeltzer SN, Faulkner C, Bronson SL, Murphy BL, Richards DA, Holland KD, and Danzer SC. 2012. 'Excessive activation of mTOR in postnatally generated granule cells is sufficient to cause epilepsy', Neuron, 75: 1022–34. [PubMed: 22998871]

Steward O, Matsudaira Yee K, Farris S, Pirbhoy PS, Worley P, Okamura K, Okuno H, and Bito H. 2017. 'Delayed Degradation and Impaired Dendritic Delivery of Intron-Lacking EGFP-Arc/Arg3.1 mRNA in EGFP-Arc Transgenic Mice', Front Mol Neurosci, 10: 435. [PubMed: 29445324]

Vazdarjanova A, McNaughton BL, Barnes CA, Worley PF, and Guzowski JF. 2002. 'Experience-dependent coincident expression of the effector immediate-early genes arc and Homer 1a in hippocampal and neocortical neuronal networks', J Neurosci, 22: 10067–71.

Wang Z, Reynolds A, Kirry A, Nienhaus C, and Blackmore MG. 2015. 'Overexpression of Sox11 promotes corticospinal tract regeneration after spinal injury while interfering with functional recovery', J Neurosci, 35: 3139–45. [PubMed: 25698749]

Williams MR, DeSpenza T Jr., Li M, Gulledge AT, and Luikart BW. 2015. 'Hyperactivity of newborn Pten knock-out neurons results from increased excitatory synaptic drive', J Neurosci, 35: 943–59. [PubMed: 25609613]

Zareen N, Dodson S, Armada K, Awad R, Sultana N, Hara E, Alexander H, and Martin JH. 2018. 'Stimulation-dependent remodeling of the corticospinal tract requires reactivation of growth-promoting developmental signaling pathways', Exp Neurol, 307: 133–44. [PubMed: 29729248]

SIGNIFICANCE STATEMENT

Deletion or knockdown of the tumor suppressor gene *PTEN* enables regenerative growth of adult CNS axons after injury, which is accompanied by enhanced recovery of function. Consequently, *PTEN* represents a potential target for therapeutic interventions to enhance recovery after CNS injury. Here we show that activity-dependent IEG induction is attenuated in PTEN-depleted neurons. These findings raise the intriguing possibility that functional recovery due to regenerative growth may be limited by the disruption of plasticity-related signaling pathways, and that recovery might be enhanced by restoring PTEN expression after regenerative growth has been achieved.

AAVshRNA-mediated PTEN knockdown in mature neurons in adult sensorimotor cortex and dentate gyrus activates mTOR and triggers *de novo* neuronal growth.

Cortical neurons lacking PTEN are activated by a learning experience (1hr exploration of a novel complex environment) as measured by IEG induction with no “hot spots” of IEG expression that might indicate seizure activity.

IEG induction due to high frequency stimulation of the cerebral cortex is attenuated in areas of PTEN knockdown.

Both learning and electrical activation strongly activate phosphorylation of ribosomal protein S6 in cortical neurons and this is preserved in areas of PTEN knockdown.

In the dentate gyrus, IEG induction in response to HFS of the perforant path is abrogated in areas of PTEN knockdown.

Synaptically-driven activation of phosphorylation of ribosomal protein S6 in dentate granule cells is attenuated whereas activation ERK1/2 phosphorylation is largely preserved.

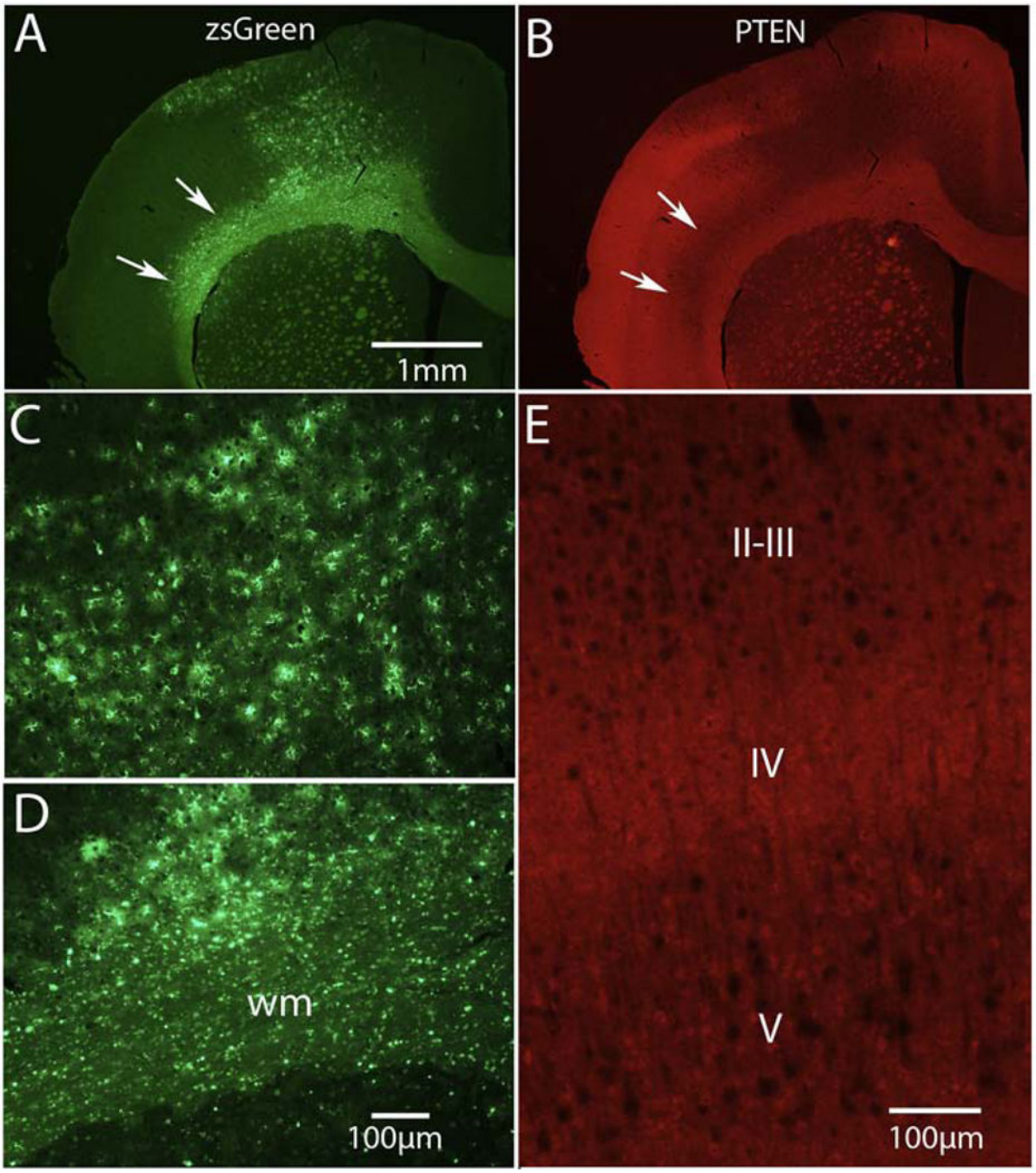

Figure 1: PTEN knockdown with intra-cortical injections of AAVshPTEN/zsGreen:
A) zsGreen fluorescence in coronal section through the sensorimotor cortex. B) Immunostaining for PTEN in the same section as in A. C) zsGreen fluorescence in gray matter in cells with astrocyte morphology. D) zsGreen fluorescence In subcortical white matter. E) Immunofluorescence for PTEN in a section 1mm caudal to the area of complete deletion. Note PTEN-negative “ghost cells” in layers II-III and layer V and preservation of PTEN expression in layer IV.

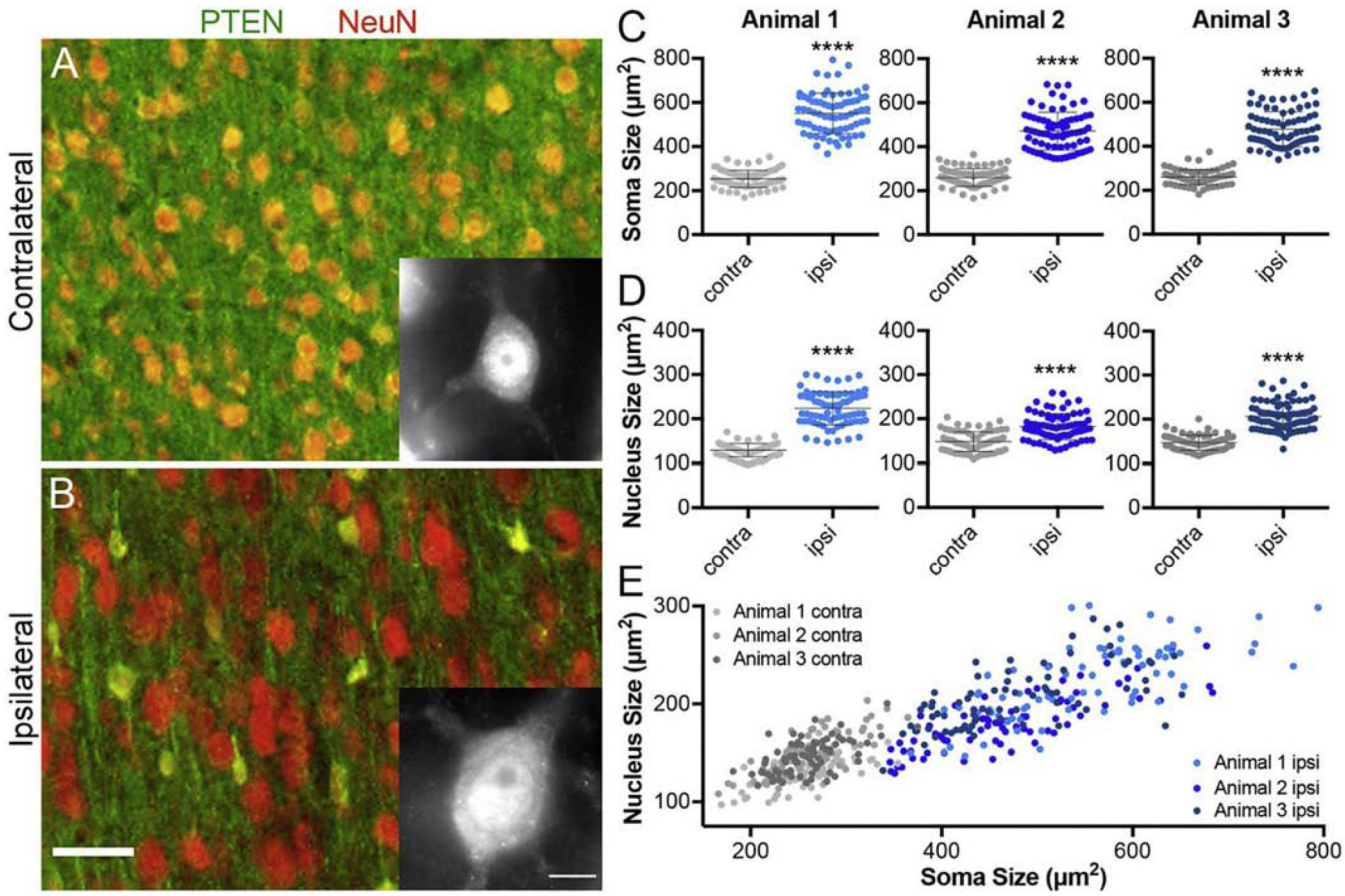

Figure 2: Enlargement of cortical neuronal cell bodies and nuclei with PTEN knockdown:

A) Immunofluorescence for PTEN (green) and NeuN (red) in the cortex contralateral to AAV-shPTEN injection. Neurons show co-localization with PTEN immunostaining. Inset represents a higher magnification image of a single PTEN-expressing neuron. B) Immunofluorescence for PTEN (green) and NeuN (red) in the area of PTEN deletion identified by the absence of immunofluorescence for PTEN. Note that all NeuN-positive neurons are PTEN-negative. Inset represents a higher magnification image of a single PTEN-depleted neuron. C) Scatter plots of soma cross-sectional areas of PTEN-depleted and PTEN-expressing neurons in three cases. D) Scatter plots of nuclear cross-sectional area of PTEN-depleted and PTEN-expressing neurons in the three cases shown in C. Paired t test comparing contralateral vs. ipsilateral side in individual rats [$p < 0.0001$]. Two-way ANOVA comparing PTEN-depleted and PTEN-expressing neurons in all rats [$F(1, 8) = 109$, $p < 0.0001$]. E) Plot of soma vs. nuclear size in the same three cases showing clear separation between PTEN-expressing and PTEN-depleted cortical neurons. Data points for each individual rat are shown in different shades of gray (for contralateral, PTEN-expressing neurons) and blue (for ipsilateral, PTEN-depleted neurons). Scale bar in A = 50μm, inset = 10μm.

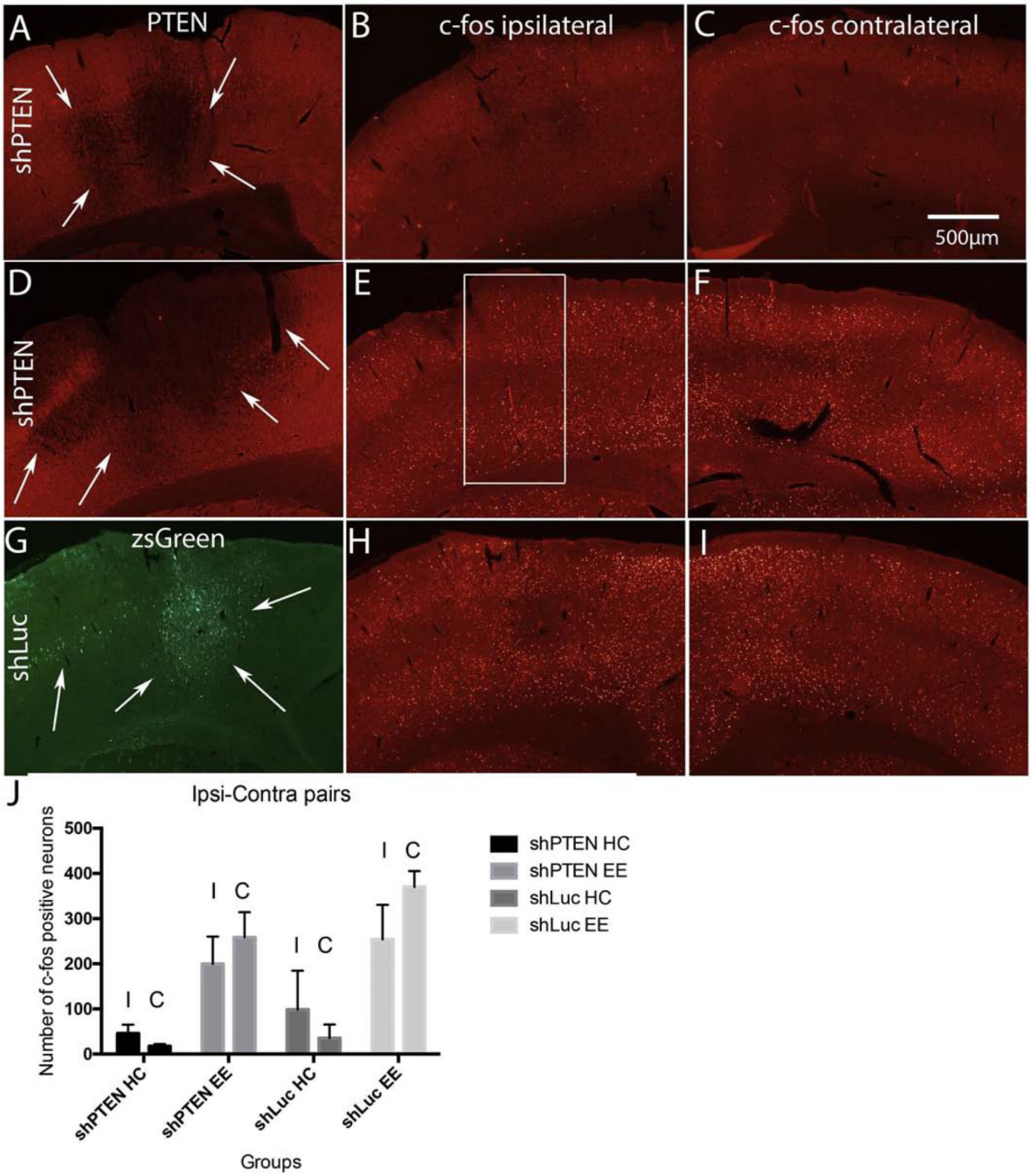

Figure 3: C-fos expression in cortical neurons in areas of PTEN knockdown:

Home cage vs. EE: A) Area of PTEN knockdown as revealed by immunofluorescence for PTEN in one rat from the HC condition; B) Immunostain for c-fos in the area of PTEN knockdown in a nearby section. C) Immunostain for c-fos on the contralateral side of the section in B. D) Area of PTEN knockdown as revealed by immunofluorescence for PTEN in one rat from the EE condition; E) Immunostain for c-fos in the area of PTEN knockdown in a nearby section. F) Immunostain for c-fos on the contralateral side of the section in E. G) Area of PTEN zsGreen fluorescence in a rat that received AAVshLuc; H) Immunostain for

c-fos in the same section shown in G. H) Immunostain for c-fos on the contralateral side of the section in G. J) Average number of c-fos positive neurons in a 750μm-wide cortical counting frame in the different groups. Two-way ANOVA comparing HC vs. EE conditions [F (3/16)=10.52, p<.0005]. Two-way ANOVA comparing PTEN depleted (ipsilateral) vs. the contralateral control [F (1/16=0.08, p=.78).

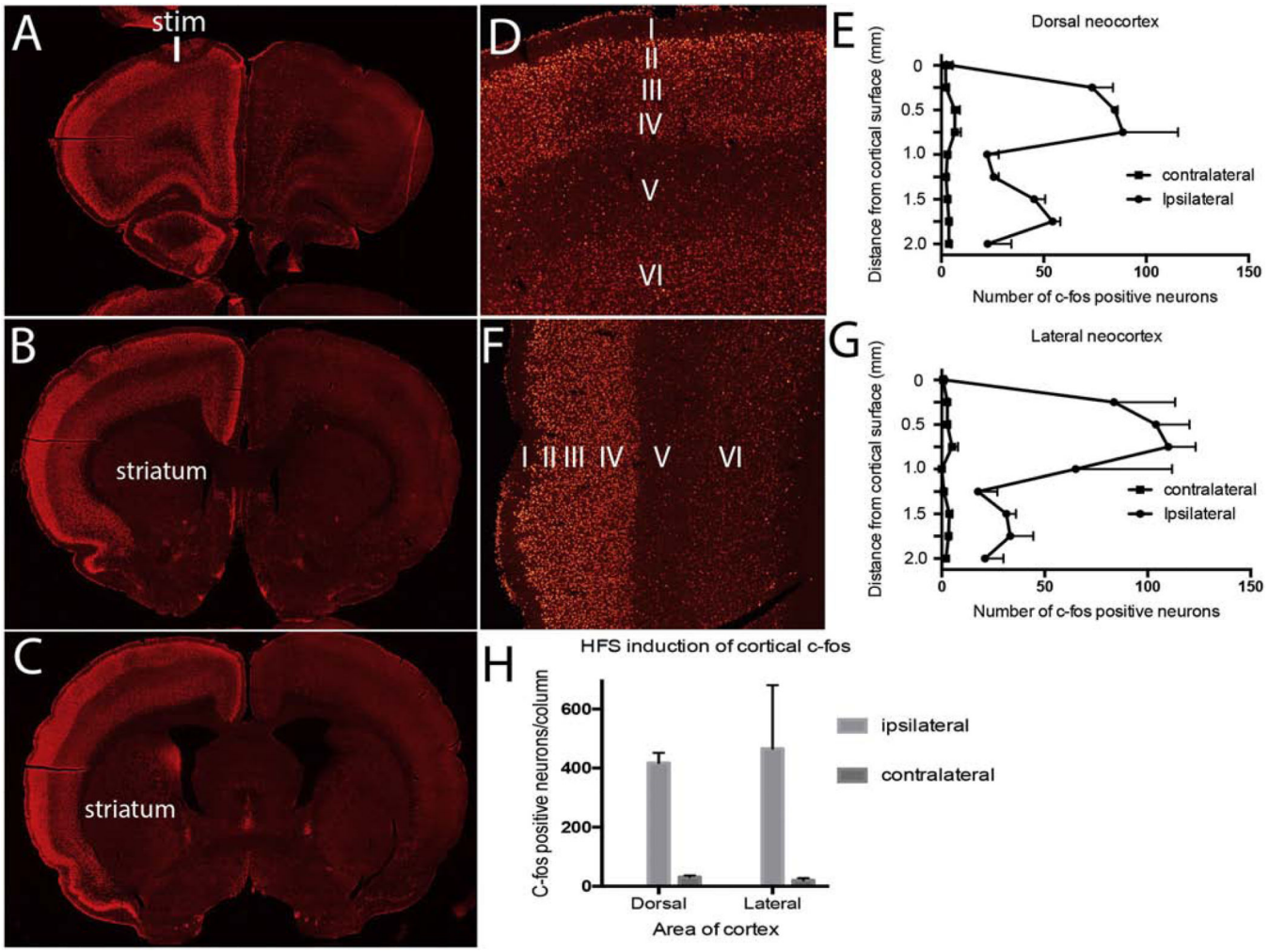

Figure 4: IEG induction following high frequency stimulation (HFS) of the cortex:

A-C) immunostaining for c-fos at different rostro-caudal levels in a rat that received HFS (20 msec trains at 400hz repeated 1/10 sec for 10 minutes). D) Pattern of c-fos labeling across cortical layers in the dorso-medial cortex (M1). E) counts of c-fos positive neurons across cortical layers in 3 rats. F) Pattern of c-fos labeling across cortical layers in the lateral cortex (S1). G) counts of c-fos positive neurons across cortical layers in the lateral cortex in 3 rats. H) Total number of neurons in a 250μm wide column (sum of counts across layers), ipsilateral vs. contralateral to the stimulation and in dorsal vs. medial cortex. Two-way ANOVA: dorsal vs. lateral cortex [$F(1,8)=0.09$, $p=0.773$, nsd]; ipsilateral vs. contralateral [$F(1,8)=43.6$, $p=0.0002$].

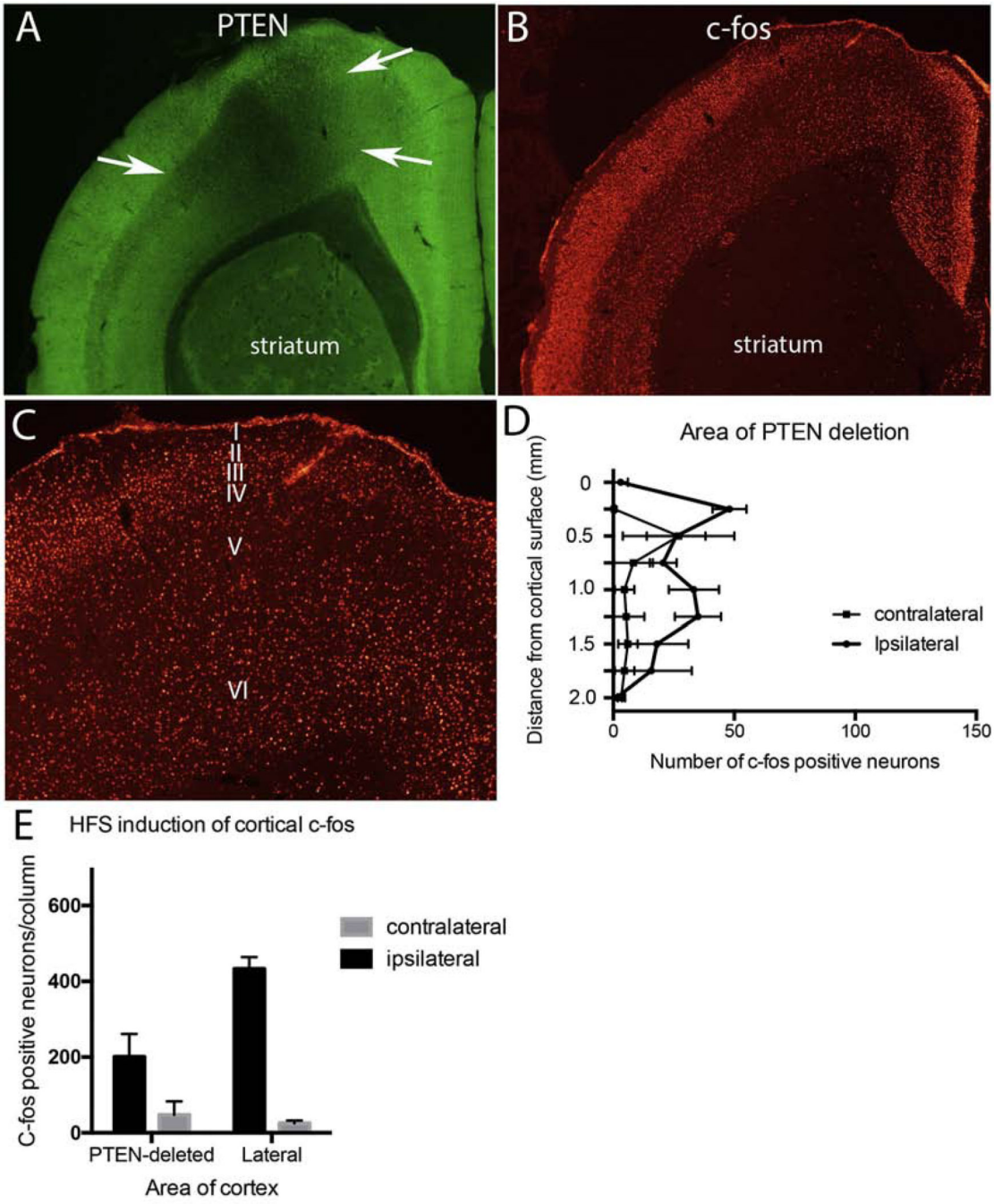

Figure 5: Induction of c-fos with cortical HFS is diminished in areas of PTEN knockdown.

A) Section from one rat immunostained for PTEN to reveal area of PTEN knockdown; B) Nearby section stained for c-fos; C) Higher magnification view of section shown in B. C) Counts of c-fos positive neurons across cortical layers in the area of PTEN knockdown (n=3 rats). D) Total number of c-fos positive neurons across layers in the area of PTEN knockdown vs. the lateral cortex. Two-way ANOVA: PTEN depleted vs. lateral cortex [$F(1,8)=22.4$, $p=0.0015$]; ipsilateral vs. contralateral [$F(1,8)=160$, $p=0.0001$].

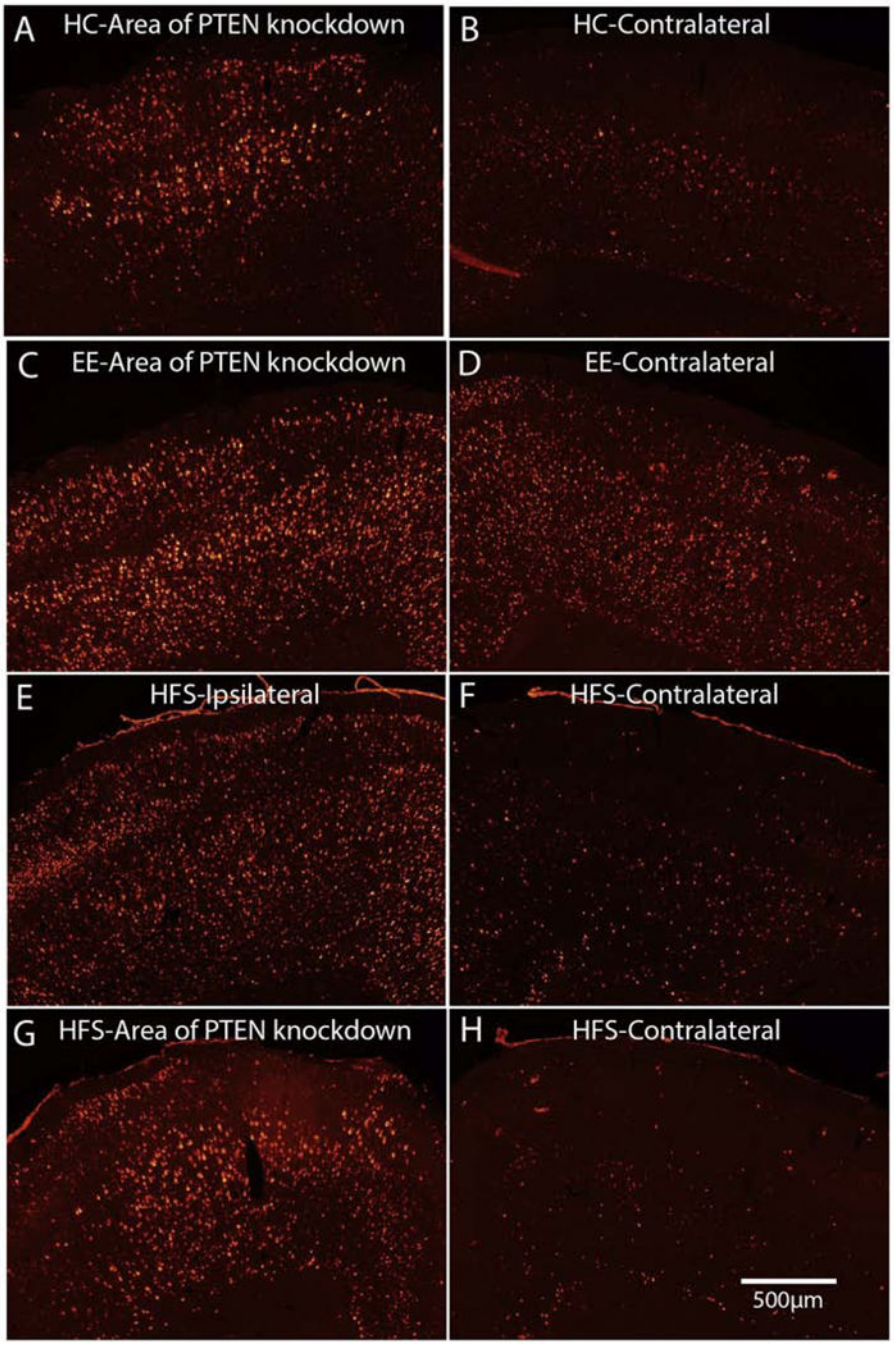

Figure 6: Induction of S6 phosphorylation with PTEN knockdown, exploration of an enriched environment, and cortical stimulation.

A) Induction of S6 phosphorylation (p-240–244) in areas of PTEN knockdown in a rat from the HC group (same case as illustrated in Fig. 3A). B) Contralateral side of the same section as in A. C) Induction of S6 phosphorylation after 1h exploration of a novel enriched environment (EE) in areas of PTEN knockdown. D) Contralateral side of the same section as in C. E) Induction of S6 phosphorylation with unilateral HFS of the cortex (same rat as illustrated in Fig. 3). F) Contralateral side of the same section as in E. G) Induction of S6

phosphorylation in areas of PTEN knockdown with unilateral HFS of the cortex. H) Contralateral side of the same section as in G. Scale bar=500μm.

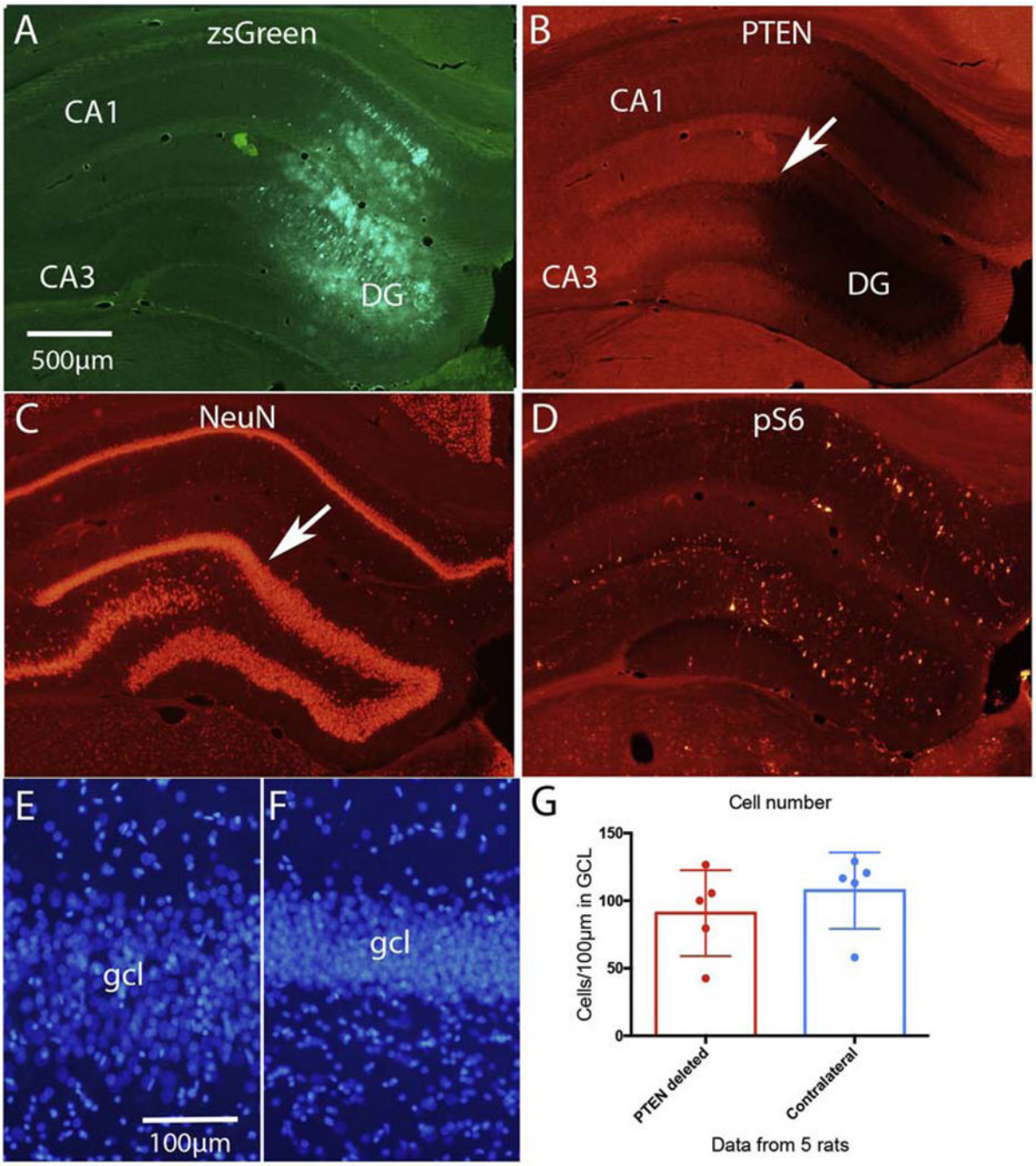

Figure 7: AAAVshPTEN injections into the dentate gyrus:

A) zsGreen fluorescence in the area of AAVshPTEN transfection. B) Immunofluorescence for PTEN reveals a focal area of PTEN knockdown 1–2 mm in diameter. Arrow indicates the boundary of the area of PTEN deletion. C) Immunofluorescence for NeuN reveals increases in cell size and thickness of the granule cell layer in the area of PTEN knockdownn. D) Immunofluorescence for phosphorylated ribosomal protein S6 (p-Ser 235/236) in the area of PTEN knockdown; note large neurons in the granule cell layer and neurons in the hilus and CA1 region. E) DAPI-stained nuclei in the granule cell layer (GCL) in the dorsal leaf in the

area of PTEN knockdown; F) DAPI-stained nuclei in the granule cell layer contralateral to the injection. G) Average number of DAPI-stained nuclei in 100μm wide columns along the granule cell layer (dorsal blade) in the area of PTEN knockdown and in the homologous region in the contralateral dentate gyrus.

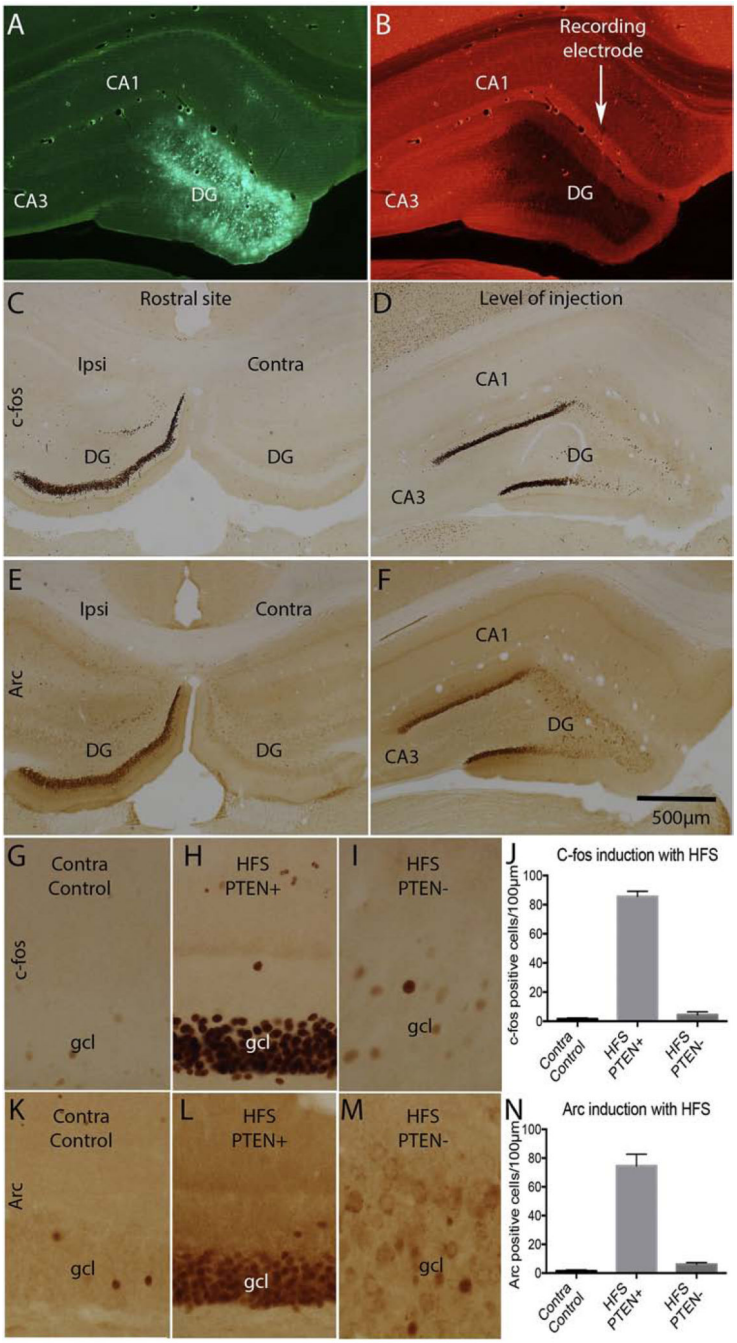

Figure 8: Abrogation of activity-dependent IEG induction in PTEN-depleted dentate granule cells:

A) Area of transfection marked by zsGreen expression. B) Immunostaining for PTEN reveals area of PTEN knockdown. Path of recording electrode is marked. C) Pattern of c-fos immunostaining in the rostral dentate gyrus distant from the site of PTEN knockdown. D) Pattern of c-fos immunostaining in the area of PTEN knockdown. E) Pattern of Arc immunostaining in the rostral dentate gyrus distant from the site of PTEN knockdown. F) Pattern of Arc immunostaining in the area of PTEN knockdown. G) High magnification view of the dorsal blade of the dentate gyrus on the side contralateral to the stimulation

where only a few granule cells express c-fos (control); H) Lateral part of the dorsal blade on the side of the high frequency stimulation where there is robust induction of c-fos in virtually every dentate granule; I) In the area of PTEN knockdown; J) Counts of c-fos-positive granule cells per 100μm length of the granule cell layer in the 3 sites illustrated in G-I. One way ANOVA (DF 2,6, $F=1207$, $p<0.0001$). K,L,M) High magnification views of Arc-positive granule cells in the same 3 sites as G-I. N) Counts of Arc-positive granule cells per 100μm length of the granule cell layer in the 3 sites illustrated in K-M. One way ANOVA (DF 2,6, $F=225$, $p<0.0001$).

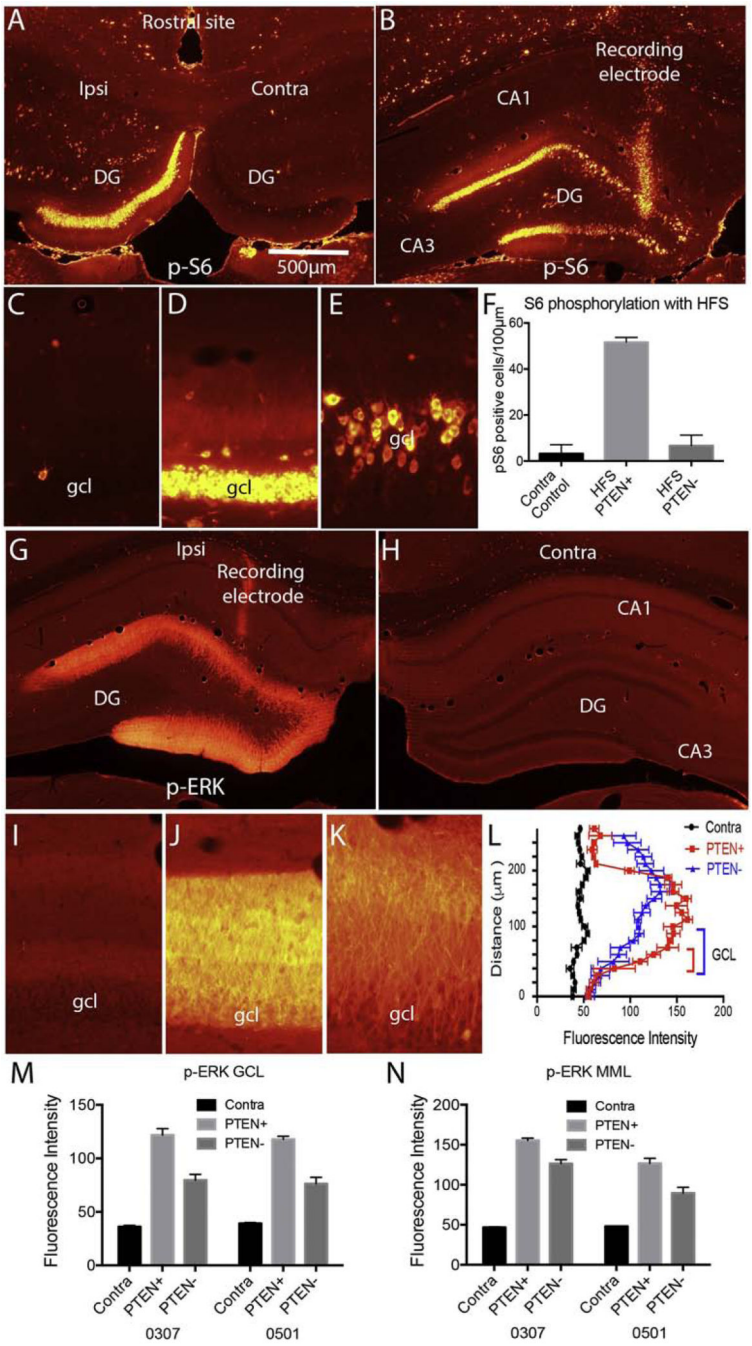

Figure 9: Attenuation of activity-dependent kinase signaling in PTEN-depleted dentate granule cells:

A) Pattern of p-S6 immunostaining in the rostral dentate gyrus distant from the site of PTEN knockdown. B) Pattern of p-S6 immunostaining in the area of PTEN knockdown. C) High magnification view of the dorsal blade of the dentate gyrus on the side contralateral to the stimulation. D) Lateral part of the dorsal blade on the side of the high frequency stimulation. E) Dorsal blade in the area of PTEN knockdown. F) Counts of p–S6-positive granule cells per 100μm length of the granule cell layer in the 3 sites illustrated in C-E. One way ANOVA (DF 2,6, F=162, p<0.0001). G) Immunostaining for p-ERK in the area of PTEN knockdown;

H) Immunostaining for p-ERK on the contralateral side of the section in G. I) High magnification view of the dorsal blade of the dentate gyrus on the side contralateral to the stimulation. J) Lateral part of the dorsal blade on the side of the high frequency stimulation. K) Dorsal blade in the area of PTEN knockdown. L) quantification of fluorescence intensity for ERK1/2 across the cell body and dendritic laminae in the areas illustrated in I-J. M) Quantification of average fluorescence intensity for p-ERK over the granule cell body layer (GCL) in 2 rats. N) Quantification of average fluorescence intensity for p-ERK over the middle molecular layer (MML).

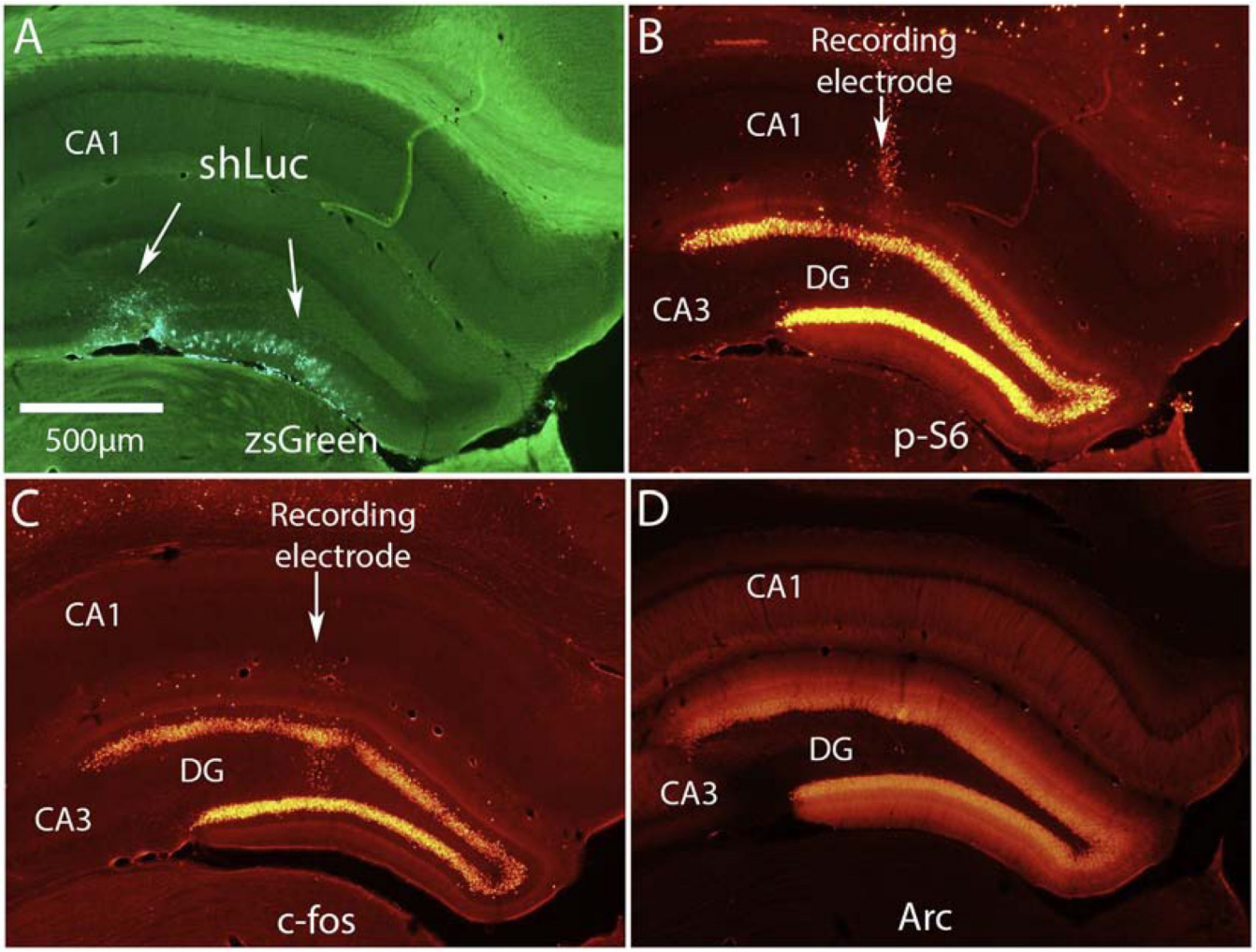

Figure 10: No effect of AAVshLuc on IEG induction and activity-dependent kinase signaling:
A) Area of transfection marked by zsGreen expression. In this case, transfection is mainly in the ventral blade of the dentate gyrus. B) Immunostaining for p–S6 in the area of AAVshLuc delivery reveals activation due to HFS of the perforant path. C) Nearby section immunostained for c-fos. D) Nearby section immunostained for Arc.